Heliyon 10 (2024) e34214

Contents lists available at ScienceDirect

Heliyon

journal homepage: www.cell.com/heliyon

Research article

The protective effects of aqueous extract of *Schisandra sphenanthera* against alcoholic liver disease partly through the PI3K-AKT-IKK signaling pathway

Ding Liu [a], Kai Yang [a], Taotao Li [a], Tiantian Tang [a], Yujiao Wang [a], Wenfei Wang [a], Jia Li [a], Peijie Zhou [a], Xuan Wang [a], Chongbo Zhao [a], Dongyan Guo [a], Yundong Xie [a], Jiangxue Cheng [a], Mei Wang [a], Jing Sun [a,*], Xiaofei Zhang [a,b,**]

[a] *Key Laboratory of Basic and New Drug Research in Chinese Medicine, Shaanxi University of Chinese Medicine, Xianyang, Shaanx, 712046, China*
[b] *Key Laboratory of Modern Chinese Medicine Preparation, Ministry of Education, Jiangxi University of Traditional Chinese Medicine, Nanchang, Jiangxi, 330004, China*

ARTICLE INFO

Keywords:
Schisandra sphenanthera
Alcoholic liver disease
UPLC-Q-TOF-MS/MS
Transcriptome sequencing
Pharmacology

ABSTRACT

Purpose: This study aimed to investigated the key chemical components and the effect of the aqueous extract of *Schisandra sphenanthera* (SSAE) on alcoholic liver disease (ALD) and the related molecular mechanism.

Methods: This study employed UPLC-Q-TOF-MS/MS to identify the chemical compositions in SSAE. ALD rat model was established through oral administration of white spirit. Transcriptome sequencing, weighted gene co-expression network construction analysis (WGCNA), and network pharmacology were used to predict key compositions and pathways targeted by SSAE for the treatment of ALD. Enzyme-linked immunosorbent assay (ELISA), biochemical kits, hematoxylin-eosin (HE) staining, Western blotting (WB) analysis, and immunohistochemical analysis were used to validate the mechanism of action of *SSAE* in treating ALD.

Results: Active ingredients such as schisandrin A, schisandrol A, and schisandrol B were found to regulate the PI3K/AKT/IKK signaling pathway. Compared to the model group, the SSAE group demonstrated significant improvements in cellular solidification and tissue inflammation in the liver tissues of ALD model rats. Additionally, SSAE regulated the levels of a spartate aminotransferase (AST), alanine aminotransferase (ALT), alcohol dehydrogenase (ADH), and aldehyde Dehydrogenase (ALDH) in serum ($P < 0.05$); Western blotting and immunohistochemical analyses showed that the expression levels of phosphorylated PI3K, AKT, IKK, NFκB, and FOXO1 proteins were significantly reduced in liver tissues ($P < 0.05$), whereas the expression level of Bcl-2 proteins was significantly increased ($P < 0.05$).

Conclusion: The active components of SSAE were schisandrin A, schisandrol A, and schisandrol B, which regulated the phosphorylation levels of PI3K, AKT, IKK, and NFκB and the expression of

Abbreviations: ALD, alcoholic liver disease; SS, *Schisandra sphenanthera*; SSAE, the aqueous extract of *Schisandra sphenanthera*; AST, Aspartate aminotransferase; ALT, Alanine aminotransferase; ALDH, Acetaldehyde dehydrogenase; ADH, Ethanol dehydrogenase; RIPA, Radio Immunoprecipitation Assay; BP, biological process; GO, gene ontology; HE, hematoxylin–eosin staining; KEGG, Kyoto Encyclopedia of Genes and Genomes; NFκB, nuclear factor kappa-beta; PPI, protein–protein interaction networks; CCs, cell compositions; MFs, molecular functions.

* Corresponding author. School of Pharmacy Shaanxi University of Chinese Medicine. Xianyang, China.
** Corresponding author. School of Pharmacy Shaanxi University of Chinese Medicine. Xianyang, China.
E-mail addresses: ph.175@163.com (J. Sun), 2051028@sntcm.edu.cn (X. Zhang).

https://doi.org/10.1016/j.heliyon.2024.e34214
Received 16 October 2023; Received in revised form 4 July 2024; Accepted 5 July 2024
Available online 6 July 2024

FOXO1 protein and upregulated the expression of Bcl-2 protein in the liver tissues of ALD rats. These findings indicate that SSAE acts against ALD partly through the PI3K-AKT-IKK signaling pathway. This study provided a reference for future research and treatment of ALD and the development of novel natural hepatoprotective drugs.

1. Introduction

Alcoholic liver disease (ALD) has emerged as a prevalent condition in the worldwide. In 2020, the World Health Organization reported that excessive alcohol consumption accounts for approximately 45 % of the global drinking population, and results in 3.3 million deaths annually [1,2]. The pathogenesis of ALD is complicated, involving the generation of reactive oxygen radicals during alcohol metabolism, which leads to heightened lipid peroxidation compromised antioxidant enzyme activity, hepatocyte death, and subsequent oxidative damage and lipid metabolism disturbances in the liver [2,3]. Unfortunately, the efficacy of current drug therapies for ALD remains unsatisfactory, often accompanied by severe adverse effects and the risk of exacerbating inflammatory conditions. Considering the limited therapeutic options, prolonged treatment duration, and significant adverse effects, there is an urgent need for novel drugs and long-term preventive dietary interventions for ALD. Notably, natural active ingredients derived from traditional Chinese medicine offer the advantages of low toxicity and minimal adverse side effects [4], presenting unique potential in the treatment of ALD. These ingredients can not only effectively alleviate ALD symptoms, but also exhibit the potential to delay disease progression to some extent, making multi-target therapy with traditional Chinese medicine a preferable approach. Additionally, the rapid growth of the Chinese medicine industry fostered increased public awareness of health, with numerous health foods gaining popularity. Therefore, the practical application of edible plant-based natural medicines for the prevention and treatment of ALD has gained considerable attention.

Schisandra sphenanthera (SS), a member of the Magnoliaceae family, is the dried, ripe fruit of Baill or *SS*. It is widely used in the treatment of liver and kidney deficiency in Yin-Yang syndrome and is renowned for its hepatoprotective activity [5],has shown promise in the long-term treatment of various liver diseases. Clinical pharmacological studies have revealed that SS contains lignan compounds, polysaccharides, volatile oils, terpenoids, amino acids, organic acids, flavonoids, and other bioactive compounds with hepatoprotective, anti-inflammatory, anticancer, antiviral, antioxidant, and detoxifying properties [6–9]. Among these constituents, lignan compounds have been identified as the primary bioactive compounds in SS. They have been reported to inhibit hepatocarcinogenesis and possess ameliorative and therapeutic effects on ALD [10,11]. SS has demonstrated effectiveness in reducing serum levels of AST and ALT, inhibiting oxidative stress, and attenuating inflammatory response [12,13], without significant hepatotoxicity. Furthermore, SS is one of the renowned herbal species with healthy food functions, and SS is commonly used in traditional health and functional foods and has enjoys widespread application in daily dietary health care. However, due to the lack of systematic studies, the pharmacological basis and mechanism of action of SS in the treatment of ALD are still unclear and require further exploration.

Focusing on the aqueous extract of *Schisandra sphenanthera* (SSAE), this study aimed to identify the key components present in SS using UPLC-Q-TOF/MS. The target and mechanism of action of SSAE in ALD induced by excessive alcohol consumption were explored through RNA-seq, WGCNA, network pharmacology, and *in vitro* experiments. Animal experiments were conducted to validate the preliminary findings, wherein an ALD rat model was developed through oral administration of white spirit. Pharmacodynamic

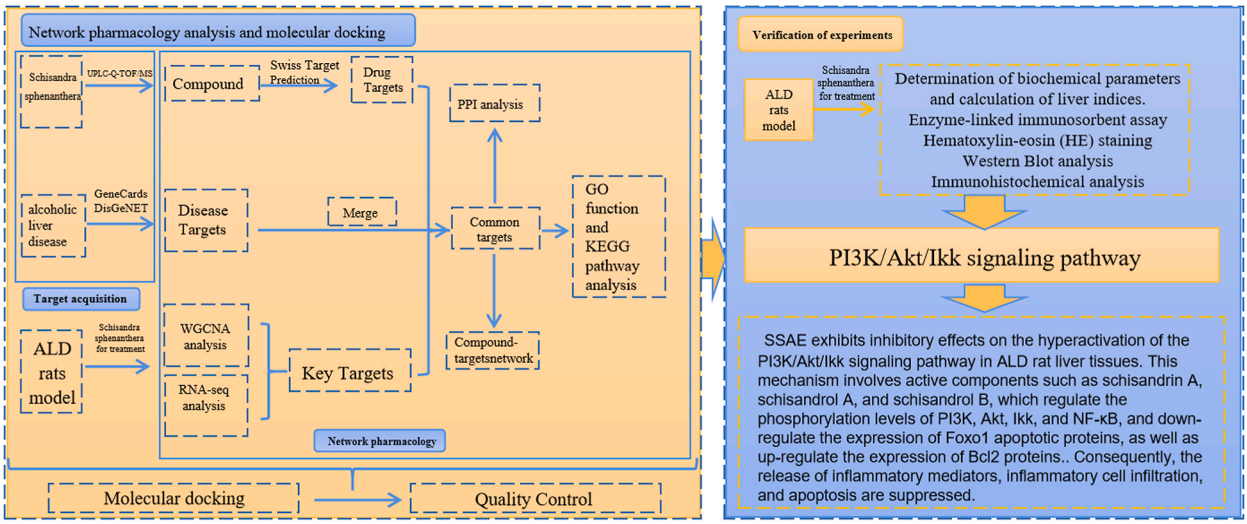

Fig. 1. Graphical abstract.

experiments involving biochemical kits, enzyme-linked immunosorbent assay kits, HE staining, protein blotting, and immunohistochemistry were employed for further validation. Consequently, a comprehensive investigation into the mechanism of action of SSAE was conducted. This study provides preliminary insights into the target and mechanism of action of SSAE in the treatment of ALD, serving as a foundation for further development and utilization of SS fruits as functional food or nutritional supplements for the prevention and treatment of ALD. The graphical abstract of the study is shown in Figure (1).

2. Materials and methods

2.1. Preparation of SSAE

The dried ripe fruit of Baill or *SS*, belonging to the family Magnoliaceae originating from Shangluo, Shaanxi Province, was purchased from Zhashui County Qinling Chinese Materia Medica Development Co. Ltd (batch number 2201001). And Professor Chang Li Wang of the Shaanxi University of Traditional Chinese Medicine verified its authenticity. First, 300g of SS herb was taken and mixed with 8 times the amount of water. The mixture was decocted for 1.5 h, filtered through a layer of gauze, and decocted three times. Three decoctions were mixed and concentrated to 300 ml to obtain SSAE.

2.2. Determination of SSAE components using UPLC-Q-TOF-MS/MS

The chemical composition of SSAE was investigated using the UPLC-Q-TOF-MS technique. An ultra-high liquid chromatograph, ACQQUITYTM UPLCC (Waters Technology, Inc., USA), coupled with a mass spectrometer, Xevo TQQ (Agilent Technologies, Inc.), was employed for the analysis. The tandem Triple TOF 6600-1 quadrupole mass spectrometer was operated in electrospray positive and negative scan modes, with a scan range of *m/z* 100 to 2000. The source voltage was set at 5500 V and −4500 V for positive and negative ions, respectively. The ion source temperature was maintained at 600 °C and 500 °C for positive and negative ions, respectively. The cracking voltage was set to ±80 V, and the collision energy was set to ±10. The total data acquisition time was 20 min. The UPLC system comprised a Waters BEH C18 column (2.1 mm × 100 mm, 1.7 μm) and a mobile phase consisting of phase A (0.1 % formic acid aqueous solution) and phase B (0.1 % formic acid/methanol/Acetonitrile). Liquid phase elution gradient was follows: 0–0.5 min, 10 % B linear; 0.5–2 min, 50 % B; 2–7 min, 80 % B linear; 7–15 min, 100 % B; 15–20 min, 10 % B. The column temperature was set at 50 °C, the volume flow rate was 0.4 mL/min, and the injection volume was 1 μL [14].

2.3. Animal experiments

Forty male (Sprague-Dawley) SD rats of SPF grade, weighing (200 ± 20) g, were purchased from Chengdu Dashuo Experimental Animal Co, Ltd. The animals were housed under controlled experimental conditions with a temperature of 25 ± 2 °C and a relative humidity of 50 ± 5 %. Prior to the experiment, the rats were acclimated and fed an appropriate diet for one week. The study was approved by the Animal Ethics Committee of Shaanxi University of Traditional Chinese Medicine (approval number SUCMDC20220530002). SD rats were randomly divided into four groups of ten rats each: control, model, positive drug, and SSAE administration groups. The positive drug was HuGanPian(KuiHua) (0.4375 g/kg/d), which contained six herbs: Bupleuri Radix, Artemisiae Scopariae Herba, Schisandrae Chinensis Fructus, Radix Isatidis, Pig Gallbladder Powder, Mung Beans [15–17]. and SSAE administration group (0.5 g/kg/d). The model, positive and SSAE administration groups were gavaged with 10 ml/kg Chinese white spirit (Beijing Red Star Erguotou, 56 %, v/v. product batch number 20220706002) for 14 consecutive days to induce the rat model of alcoholic liver disease (ALD) [18–21]. The SSAE administration group was gavaged 0.05 g/ml of SSAE solution for 14 days prior to white spirit administration [18,22], with a time interval of 1h. At the end of the experiment, all rats were anesthetized with 2.5 % uratan solution and euthanized. Rat livers were collected, immediately frozen in liquid nitrogen, and subsequently preserved in a −80 °C refrigerator for further analysis.

2.4. RNA-seq analysis

Four rat liver tissues were randomly selected from each of the control, model and SSAE groups for total RNA extraction and mRNA enrichment [23]. Reverse transcription into double-stranded cDNA, repair of cDNA double-ends, the addition of connectors, and PCR amplification were performed to construct an online library. Bioinformatics analysis was performed using Omicsmart (http://www.omicsmart.com), an interactive online data analysis platform. Differential gene expression analysis was conducted with a significance threshold of FDR$<$0.05 and log2|FC|$\geq$2. Additionally, Gene Ontology (GO) and KEGG Pathway enrichment analyses were performed based on the results of the differential gene expression analysis [24].

2.5. Weighted gene co-expression network construction analysis (WGCNA) and detection of gene modules

After removing outlier samples and based on platform analysis conditions, the relationship between gene regulatory networks was determined. Pairwise correlation matrices were generated for all DEGs, and topological overlap measures were used to detect hierarchical clusters for module identification and dendrogram creation. Correlation and clustering analyses were conducted between modules, between genes and modules, and between samples and modules, Module-trait relationship analysis was performed to assess the association between module signature genes (MEs) and phenotypes (MMs). The significant modules were determined based on the

relationship with AST, ALT, ADH, and ALDH. Trait-associated genes were further investigated within the module, and the gene significance value (GS) was calculated by measuring the Pearson correlation between each gene and the trait data. Key genes within the modules were selected to construct the protein-protein interaction (PPI) network. Finally, GO enrichment and KEGG pathway enrichment analyses were conducted for the genes within the modules [23,24].

2.6. Component-target-based network pharmacology analysis

2.6.1. Acquisition of SSAE component targets and ALD targets

The component targets of SSAE were identified using the PubChem (http://pubchem.ncbi.nlm.nih.gov/) database, the Swiss Target Prediction database, and the Meta target database. To obtain the relevant target genes associated with ALD, Genecards (https://www.genecards.org/), DisGennet (https://www.Disgenet.org/), and OMI(https://omim.org/) databases were searched with, the keyword “alcohol liver disease", which were then integrated and defined [25].

2.6.2. Network construction and GO/KEGG enrichment analysis of ALD-SSAE components

The active ingredients of SSAE, ALD targets, and RNA-seq differential gene targets were imported into the online Venny diagram platform (http://bioinformatics. psb. ugent. be/webools/venn) to obtain the key targets of SSAE active ingredients in treating ALD. The SSAE component targets were imported into Cytoscape 3.7.2 software (http://www.cytoscape.org/) to construct the SSAE component-target network. The network was filtered based on the degree size to determine the interaction relationship and importance between active components of SSAE and disease-related targets. The collated cross-target genes were then imported into the String database (http://string-db.org), with the study species as “Homos Sapiens" and a confidence level of 0.7, thus obtaining the PPI network map [26]. The EnsembLID and log2fc of the intersecting genes were used for KEGG and GO enrichment analyses using R software [27,28].

2.7. Molecular docking prediction

The key targets of the PI3K/AKT pathway were molecularly docked to their corresponding components to predict their interactions. Based on the screening of enriched targets on the pathway, PDB structure files of PIK3CA, TNF, AKT1and IKK target proteins were downloaded from the RSCB-PDB database, whereas SDF format files of the corresponding components were downloaded from the PubChem database. The target proteins and compound structure files were imported into Discovery Studio 4.5 software and subjected to molecular docking using the LibDock module.4.5 software.

2.8. Quality control of SSAE

Based on the 2020 edition of the Chinese Pharmacopoeia, combined with the results of network pharmacology and molecular docking prediction, we selected three components of Schisandrol A, Schisandrol B, and Schisandrin A were selected as the quality control standard samples Then, high performance liquid chromatography (HPLC) was used to identify the main active ingredients in SSAE and for quality control. Firstly, 2 ml of SSAE solution was diluted to 8 ml with methanol, sonicated (power 250W, frequency 40 kHz) for 30min, and cooled. Methanol was added to make up for the lost volume, and the tubes were shaken well. The filtrate was then passed through a 0.22 μm microporous membrane to obtain the test solution. The sample solution was weighed into a 10 ml volumetric flask, dissolved in methanol, shaken well, and sonicated (power 250W, frequency 40 kHz) for 10min, and finally calibrated to obtain the mixed control solution. The chromatographic analysis was performed on an Agilent TC-C18 column (4.6 mm × 250 mm, 5 μm). A gradient of the mobile phase (phase A: acetonitrile, phase B: water) was used, as detailed in Table 3. The detection wavelength was set at 252 nm, the volumetric flow rate was 1 mL/min, the column temperature was 30 °C, and the injection volume was 10 μL was [29]. The identification of schisandrol A, schisandrol B, and schisandrin A in the SSAE samples was accomplished by comparing and analyzing the peak retention times between the test and standard samples.

2.9. Pharmacodynamic experiments

2.9.1. Animal model preparation and grouping

The molecular mechanism of SSAE on ALD was explored, and the dose dependence of SSAE on ALD rats was investigated. Therefore, sixty male SD rats of SPF grade, weighing (200 ± 20) g, were purchased from Chengdu Dashuo Experimental Animal Co, Ltd. and acclimatized under controlled experimental conditions (temperature: 25 ± 2 °C, relative humidity: 50 ± 5 %) for 1 week. The study protocol was approved by the Animal Ethics Committee of Shaanxi University of Traditional Chinese Medicine (approval number SUCMDC20220530002). The SD rats were randomly divided into six groups, each consisting of ten animals, which were control group, model group, SSAE high dose group (1.0 g/kg/d), SSAE middle dose group (0.5 g/kg/d), SSAE low dose group (0.25 g/kg/d), and positive drug group. The positive drug was HuGanPian(KuiHua) (0.4375 g/kg/d), which contained six herbs: Bupleuri Radix, Artemisiae Scopariae Herba, *Schisandrae Chinensis Fructus*, Radix Isatidis, Pig Gallbladder Powder, Mung Beans [15–17]. Except for the control group, all the groups were gavaged with 10 ml/kg white spirit (Beijing Red Star Erguotou, 56 %, v/v. product batch number 20220706002) to develop the rat model of ALD. The gavage was administered 1h before gavage white spirit for 14 days.

2.9.2. Sample collection

After 14 days of administration, rats were anesthetized with 2.5 % uratan, and 5 mL of blood was collected from the abdominal aorta. The blood was then centrifuged at 4 °C for 10 min at 3000 r/min to separate the serum. Subsequently, the rats were euthanized. Rat livers were obtained and washed with saline. The livers were weighed, with half of them fixed in 4 % paraformaldehyde fixative, and the other half frozen in liquid nitrogen and rapidly transferred to a −80 °C refrigerator for storage.

2.9.3. Determination of biochemical parameters and calculation of liver indices

All biochemical analyses were conducted using kits purchased from the Nanjing Jiancheng Institute of Biological Engineering (Nanjing, China). The kits were used according to the instructions, and the absorbance (OD) values were measured at a wavelength of 510 nm wavelength using a microplate reader. The serum levels of aspartate aminotransferase (AST) and alanine aminotransferase (ALT) were calculated. The liver index was calculated based on the body weight and liver weight of the rats using the following formula:

$$\text{Liver index}\ (\%) = \text{liver mass}\ (\text{g})/\text{body mass}\ (\text{g}) * 100\%.$$

2.9.4. Enzyme-linked immunosorbent assay

The content of alcohol dehydrogenase (ADH) (batch number: MM-019R1) and aldehyde dehydrogenase (ALDH) (batch number: MM-0180R1) in each group of rats was determined using ELISA. A double antibody one-step sandwich enzyme-linked immunosorbent assay was performed according to the kit instructions. The OD values were measured at 450 nm using a microplate reader, and the standard curve was plotted to calculate the content of ADH and ALDH in the samples.

2.9.5. Hematoxylin-eosin (HE) staining

Liver tissues fixed in 4 % paraformaldehyde and embedded in paraffin were sectioned into 5 μm thick sections, stained with hematoxylin-eosin (HE) and examined pathologically under a 200x light microscope (OLYMPUS Japan).

2.9.6. Western blotting analysis

Total proteins were extracted from liver tissue using RIPA lysis buffer (Solarbio item No. FD008). Protein concentrations were determined using BCA assay (Bevotime). Equal concentrations were separated by sodium dodecyl sulfate-polyacrylamide gel electrophoresis and electrotransferred onto polyvinylidene difluoride (PVDF) membranes (Amersham). After blocking with 5 % bovine serum albumin, the membranes were labeled with primary antibody overnight at 4 °C and probed with HRP-coupled secondary antibody HRP-Goat anti Rabbit (Proteintech, item number SA00001-2). After exposure to x-ray film, protein bands were visualized on an enhanced chemiluminescence (ECL) detection system (Amersham), and the target bands were analyzed with a gel image processing system to analyze and calculate the relative expression of the target protein. The antibodies in the study included anti-antibodies β-Actin (Abcam: item no. 66009-1-Ig), anti-AKT (Proteintech, item no. 10176-2-AP), anti p-AKT (Abcam, item no. AB192623), anti-IKKα (Proteintech, item no. 15649-1-AP) and anti p-IKKα (Affinity, item no. AF3010), anti-PI3K (Proteintech, item no. AF6241), anti-p-PI3K (Proteintech, item no. AF3242), anti-NFκB (Proteintech, item no. 10745-1-AP), anti-p-NFκB (Proteintech, item no. AF2006), anti-FOXO1 (Proteintech, item no. 18592-1-AP), and anti-β-Actin (Proteintech, item no. 66009-1-Ig).

2.9.7. Immunohistochemical analysis

Rat liver tissues were embedded in paraffin and sectioned after an-tigen repair, followed by endogenous peroxidase blocking, primary antibody addi-tion, and overnight incubation at 4 °C. The sections were kept at room temperature for 40 min, washed thrice with PBS for 3 min each, and incubated with HRP-labeled secondary antibody (rabbit antibody) for 60 min at 37 °C. These sections were then washed thrice with PBS for 3 min each, stained with DAB, rinsed with tap water, and re-stained with hematoxylin. The sections were sealed and photographed after dehy-dration and transparency was achieved. Three high-magnification fields were randomly selected from each section to measure the optical density of the positive cells using Image-Pro Plus 6.0 image analysis software.

2.9.8. Statistical analysis

All experimental data were analyzed using GraphPad Prism Software (version 8.0.2, https://www.graphpad.com/). The results are expressed as mean ± standard error of the mean (SEM). Statistical significance was determined by one-way (ANOVA) and unpaired two-tailed Student's *t*-test. The statistical significance level was set as ($^*p < 0.05$).

3. Results

3.1. Results of UPLC-Q-TOF-MS/MS analysis

Chemical components reported for SS were compiled by searching databases such as Chinese National Knowledge Infrastructure, PubMed, and SciFinder. A database of SSAE-related chemical components was established, containing compound names, chemical formulas, ionic modes, structural formulas, and other information according to the method under 1.2. The primary chemical components in SSAE were identified based on their relative retention times (tR), excimer ion peaks, secondary fragments, and other information. The NIST 2017, NIST E&L_HR-MS/MS_1.0, TCM Library 1.0, and TCM MS/MS Libraries were used as the matched libraries

for the SSAE. The chemical composition results are shown in Table 1. A total of 24 compounds were identified from SSAE in negative and positive ion modes, as shown in Figure (2a) and Figure (2b). The 2D structure of 24 the chemical components are shown in Figure (3a-3x).

3.2. Results of RNA-seq analysis

Using the Kidio Bio online analysis platform, a false discovery rate (FDR) of ≤0.05 and a difference multiplier of 1 were set, The PCA results are shown in Figure (4a), and the total number of DEGtargets was 946. Among them, there were 553 upregulated genes and 393 downregulated genes in the control group compared to those in the model group. The volcano plot of DEG expression is presented in Figure (4b), and the DEG heat map is shown in Figure (4c). KEGG and GO enrichment analyses were conducted for the two groups of DEGs in the control and model groups. Pathways associated with ALD were analyzed, and the enriched KEGG pathways included the PI3K-AKT signaling pathway, hepatitis B, TNF signaling pathway, inflammatory mediator regulation of TRP channels, Wnt signaling pathway, and other pathways as shown in Figure (4d). GO enrichment analysis encompassed biological process (BP), cellular component (CC), and molecular function (MF). The biological processes involved are shown in Figure (4e). GSEA-KEGG results indicated enriched pathways such as PI3K/AKT signaling pathway, NFκB signaling pathway, TNF signaling pathway, basal cell carcinoma, homologous recombination, and others, as shown in Figure (4f). GSEA-GO results demonstrated the involvement of pathways

Table 1
UPLC-Q-TOF-MS/MS analysis of chemical components of SSAE.

NO	tR/min	Identifification	Formula	Selectedion	Calculated Mass	MeasuredMass	δ/ppm	Fragmentation
1	3.57	$C_9H_{11}NO_2$	Phenylalanine	$[M+H]^+$	166.086	166.0859	−1	113.0538 [46]
2	4.87	$C_{30}H_{26}O_{12}$	Procyanidin B2	$[M+H]^+$	579.15	579.1494	−0.6	579.1463 [47]
3	5.15	$C_{15}H_{10}O_5$	Genistein	$[M+H]^+$	271.06	271.0597	−1.4	271.206, 152.0650 [48]
4	5.3	$C_{26}H_{28}O_{14}$	Schaftoside	$[M+H]^+$	565.155	565.1556	0.8	563.142, 391.0842 [49]
5	5.62	$C_{27}H_{30}O_{16}$	Rutin	$[M+H]^+$	611.161	611.1644	6.1	611.211, 303.0522 [49]
6	5.7	$C_{28}H_{34}O_{15}$	Neohesperidin	$[M-H]^-$	609.182	609.1788	−6	342.999, 301.0726 [50]
7	5.7	$C_{28}H_{34}O_{16}$	hesperidin	$[M-H]^-$	609.182	609.1788	−6	449.312, 303.0496 [50]
8	5.75	$C_{22}H_{22}O_{10}$	calycosin-7-o-glucoside	$[M+H]^+$	447.129	447.1281	−1	285.076, 270.051, 253.0492 [51]
9	5.75	$C_{22}H_{22}O_{10}$	Glycitin	$[M+H]^+$	447.129	447.1281	−1	285.0757 [52]
10	5.78	$C_{21}H_{20}O_{12}$	HyperinI	$[M+H]^+$	465.103	465.103	0.5	303.051, 285.0746 257.0387 [53]
11	6.09	$C_{15}H_{10}O_3$	Luteolin	$[M+H]^+$	287.055	287.0547	−1	287.0568 153.0232 [54]
12	6.09	$C_{15}H_{10}O_6$	Kacmpferol	$[M+H]^+$	287.055	287.0547	−1	226.1016 153.0282 [55]
13	6.14	$C_{21}H_{20}O_{11}$	Quercitrin	$[M+H]^+$	449.108	449.1074	−1	449.3126 303.0496 [56]
14	6.72	$C_{22}H_{22}O_9$	Ononin	$[M+H]^+$	431.134	431.1333	0.7	269.0814 254.0588 [57]
15	6.78	$C_{27}H_{42}O_4$	Ruscogenin	$[M+H]^+$	431.316	431.319	7.9	431.252 [58]
16	7.25	$C_{16}H_{12}0_5$	Calycosin	$[M+H]^+$	285.076	285.076	0.8	270.0515 253.0492 225.055, 213.0545 [59]
17	9.75	$C_{24}H_{32}O_7$	Schizandrol A	$[M+H]^+$	433.222	433.2231	2.4	384.1951 346.1417 369.1719 [60,61]
18	9.75	$C_{26}H_{30}O_7$	Betulinicacid	$[M+H]^+$	455.206	455.2048	−3.6	455.2051 [59]
19	10.54	$C_{27}H_{42}O_3$	Diosgenin	$[M+H]^+$	415.321	415.3199	−2.6	269.0813 [60]
20	10.61	$C_{23}H_{28}O_7$	Schizandrol B	$[M+H]^+$	417.191	417.1917	2.2	399.1824 369.173, 285.0770 [58]
21	11.14	$C_{23}H_{30}O_6$	Schisanhenol	$[M+H]^+$	403.212	403.2118	0.6	302.1173 [58]
22	11.25	$C_{30}H_{32}O_7$	Schisantherin A	$[M+H]^+$	537.212	537.2105	−2.7	437.159, 415.177, 371.151, [58],
23	12.23	$C_{24}H_{32}O_6$	Schisandrin A	$[M+H]^+$	417.227	417.2276	1	402.203, 301.1076 [57,61]
24	13.29	$C_{10}H_{10}O_3$	Daphnetin	$[M+H]^+$	179.07	179.0697	−3.2	179.074, 113.0642 [61]

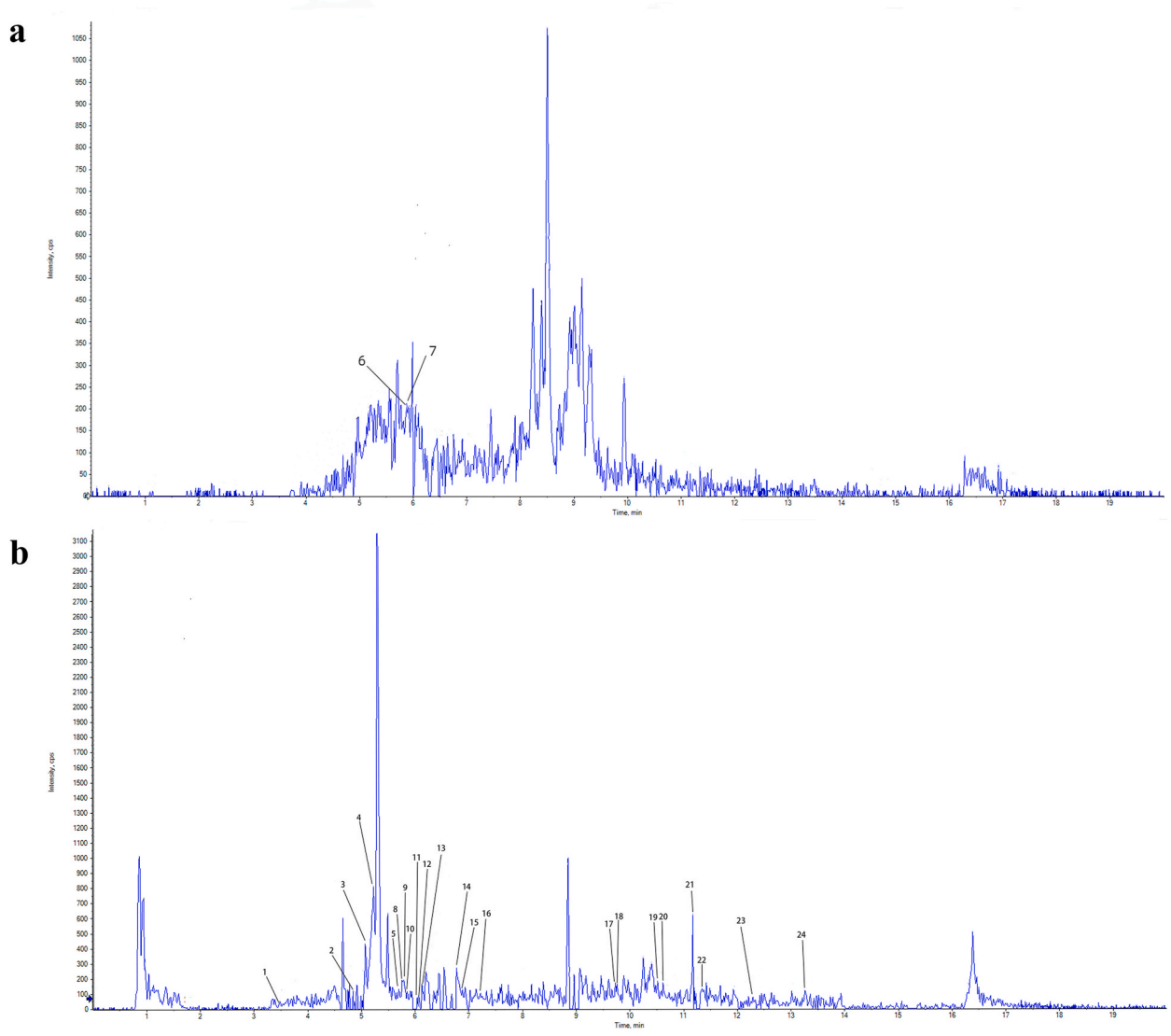

Fig. 2. Total ion flow chromatogram of SSAE.
Note:(a) Negative ion diagram. (b) Positive diagram.

related to odorant binding, transposition RNA-mediated, extracellular matrix structural constituent, acellular matrix component, and others, as depicted in Figure (4g).

3.3. WGCNA results

WGCNA was conducted using the Kidio Bio online analysis platform. Firstly, we clustered the results of the hierarchical clustering of all sample processes based on the expression of all genes as shown in Figure (5a); Then, the minimum power value of 0.8 was set the scale-free topological fit for constructing the network. The scale independence and average connectivity of different modules were evaluated within a power values range of 1–20, as illustrated in Figure (5b); The results of 13 modules obtained by mean hierarchical clustering and dynamic tree cropping are shown in Figure (5c). The correlation results between the two modules are shown in Figure (5d), where a darker square indicates a stronger correlation and a lighter square indicates a weaker correlation. The correlation analysis between gene expression and module eigenvalues is shown in Figure (5e), with darker colors indicating stronger connectivity between corresponding genes in the row and column. Figure (5f) displays the correlation analysis results of gene expression in key modules across different samples, with red representing high expression and green representing low expression. The results of data correlation between module eigenvalues and specific traits and phenotypes are shown in Figure (5g), with red representing positive correlation and green representing negative correlation, where a darker color indicates a stronger correlation. The number in brackets represents the significance P-value, with a smaller value, indicating a stronger significance. Pearson correlation results between each

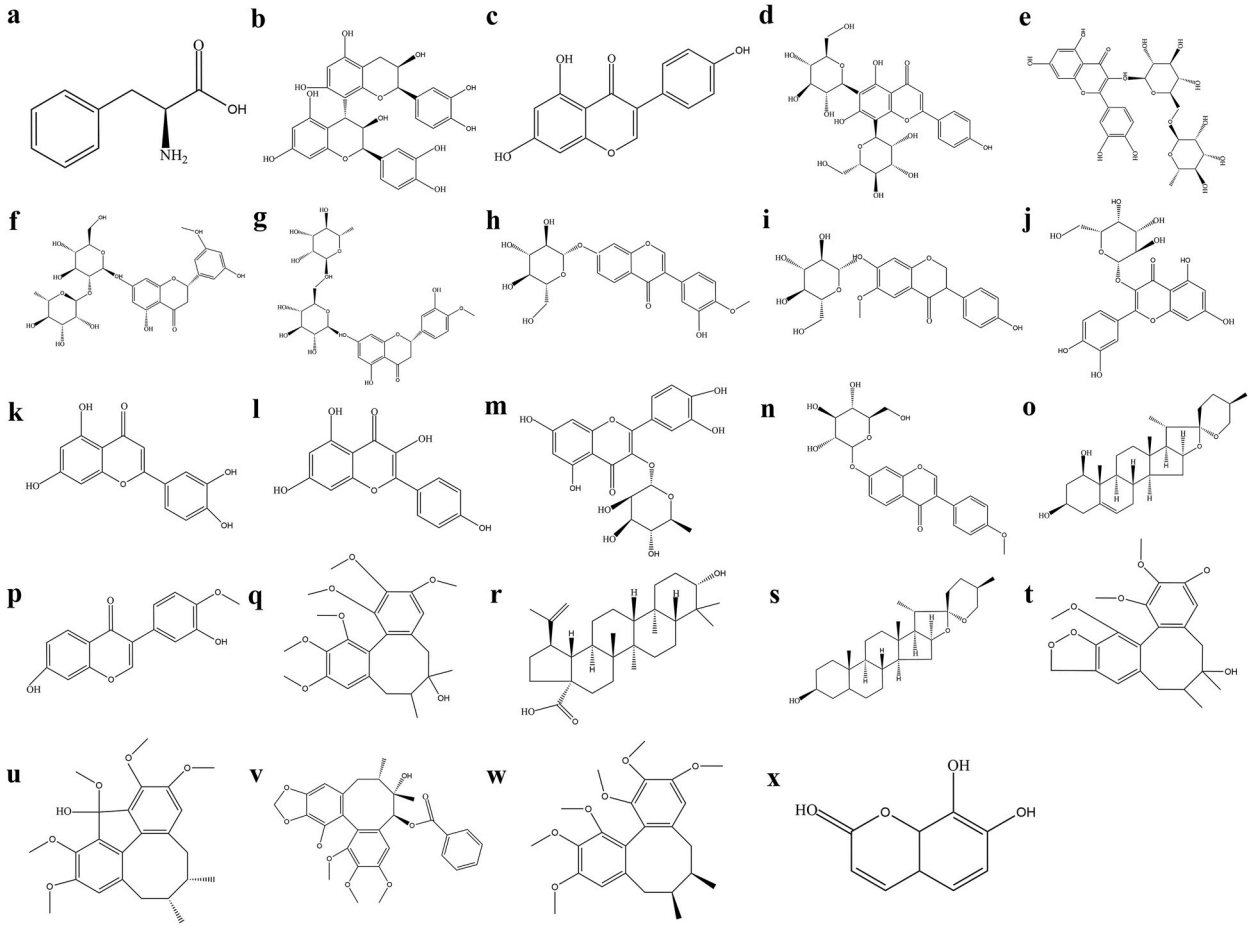

Fig. 3. Structural demonstration of the chemical composition of SSAE.
Note:(a) Phenylalanine. (b) Procyanidin B2. (c) Genistein. (d) Schaftoside. (e)Rutin. (f) Neohesperidin. (g) Hesperidin. (h) Calycosin-7-o-glucoside. (i) Glycitin. (j) Hyperin. (k) Luteolin. (l) Kacmpferol. (m) Quercitrin. (n) Ononin. (o) Ruscogenin. (p) Calycosin. (q) Schizandrol A. (r) Betulinic acid. (s) Diosgenin. (t) Schizandrol B. (u) Schisanhenol. (v) Schisantherin A. (w) Schisandrin A. (x) Daphnetin.

gene and trait data under the key module are presented in Figure (5h), with higher GS values, indicating greater significance of the gene of the corresponding phenotype trait. Figure (5i) shows the expression of genes in the key module across different samples, with red indicating upregulation and green indicating downregulation. The gene co-expression network in the key module is visualized in Figure (5j), where each point in the graph represents a gene. Darker and larger nodes indicate higher abundance and stronger connectivity. KEGG enrichment analysis results indicate enrichment in pathways such as PI3K/AKT signaling pathway, NFκB signaling pathway and others as displayed in Figure (5k). GO enrichment analysis of key module genes was performed in terms of BP, CC, and MF. The biological processes involved are shown in Figure (5l).

3.4. Network construction and GO function and KEGG pathway enrichment analyses

A total of 799 targets for SSAE were identified using PubChem, Swiss Target Prediction, and Meta Tar Fisher databases. Additionally, 6004 targets for ALD were obtained from GeneCards, DisGeNet, and OMIM databases. The intersection of SSAE component targets, ALD targets, and sequenced DEGs resulted in 26 targets of SSAE associated with insomnia as shown in Figure (6a). To visualize the relationships between components and genes, the intersecting gene target data were imported into Cytoscape 3.7.2 software, facilitating the construction of a “component-target" network map of SSAE for the treatment of ALD. The results are shown in Figure (6b), where the yellow circles represent the key genes and the blue diamonds represent the active components of SSAE, with connecting lines indicating the relationship between components and genes. The PPI network was constructed by importing 26 intersecting genes into STRING, the results of which are shown in Figure (6c). The PPI network consisted of 26 nodes, with IKBKB, AKT1 and TNFRSF1A, identified as key targets of SSAE for the treatment of ALD. These genes played a crucial role in the treatment of ALD and were selected based on their degree centrality values. The Ensembl ID and log2fc values of the 26 intersecting genes were subjected to KEGG and GO enrichment analyses. The KEGG enrichment analysis results, presented in Figure (6d), revealed the involvement of pathways including PI3K-AKT, TNF and FOXO signaling pathways. GO enrichment analysis results are displayed in

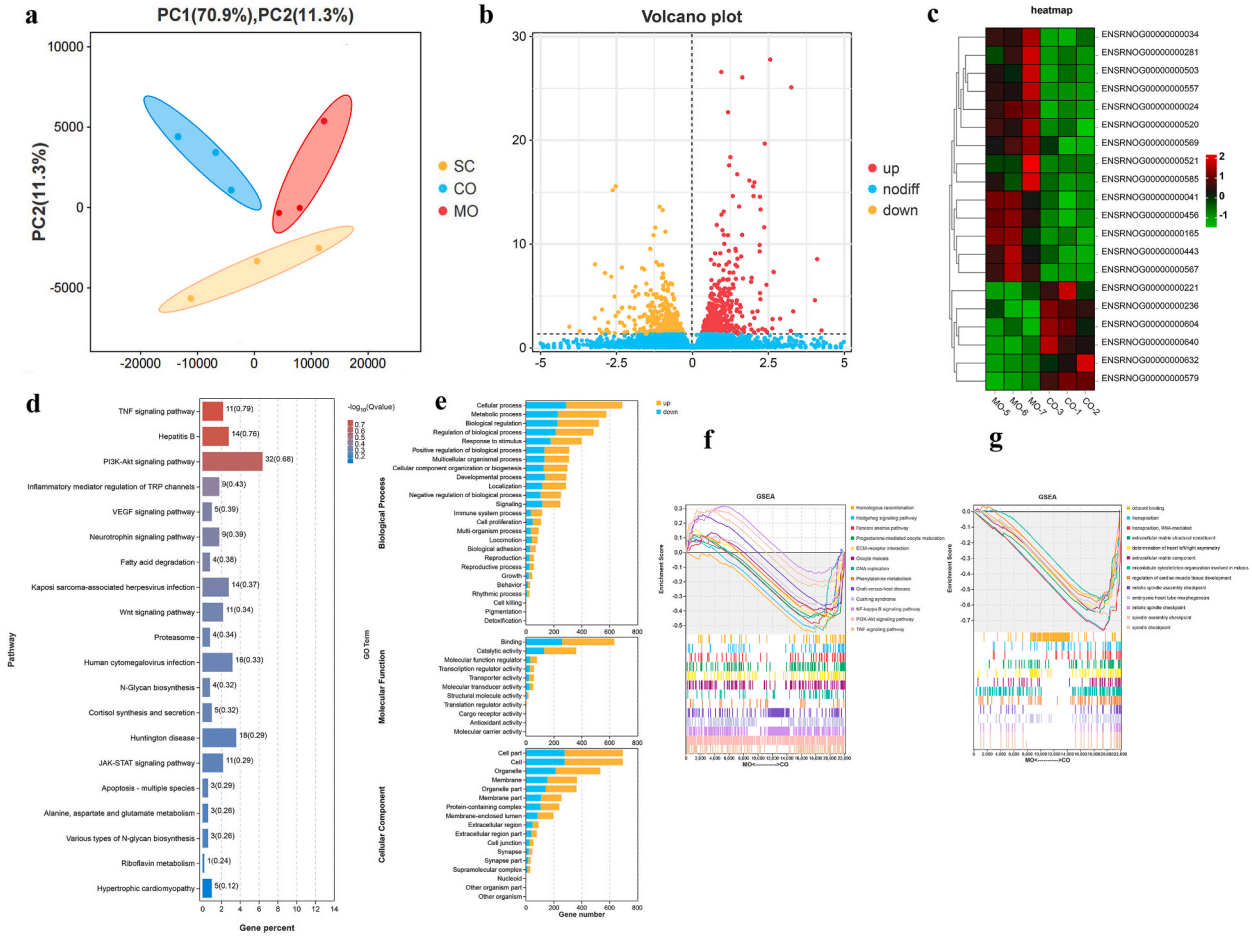

Fig. 4. Graph of RNA-seq analysis results.
Note: The PCA of gene expression is shown in (a). The volcano plot of differential gene expression is presented in (b). The differential gene heat map is shown in (c). KEGG enrichment analyses were conducted for differential genes in (d). GO enrichment analysis were conducted for differential genes in (e). GSEA-KEGG results as shown in (f). GSEA-GO results as depicted in (g).

Figure (6e). Furthermore, GO and KEGG enrichment analyses were also performed on 26 genes using R software, encompassing 25 biological processes, 17 cellular components, and 11 molecular functional pathways. The analysis revealed significant enrichment of 25 KEGG pathways. These pathways included PI3K/AKT and apoptosis signaling pathways, as shown in Figure (6f).

3.5. *Molecular docking results*

Based on the results of transcriptome sequencing, WGCNA, PPI network and KEGG enrichment analysis mentioned above, we finally obtained the key pathway of PI3K/AKT signaling pathway for ALD treatment and identified the four key target proteins IKK, AKT1, TNF and PIK3CA in the pathway. Subsequently, the active ingredients corresponding to these key targets were selected for molecular docking analysis, along with Ertiprotafib, Vatalanib, Fostamatinib, and Copanlisib as positive control drugs. Docking simulations were performed using the libdock module in Discovery Studio, and the binding affinity was assessed by the free binding energy. The molecular docking results are shown in Figure (7), and indicates the interactions between the key targets and their corresponding compounds. The interaction of PIK3CA and Schisandrin A, Schisandrol A and Schiandrol B are shown in Figure (7a-7c), the interaction of AKT1 and Schisandrol B is shown in Figure (7d), the interaction of IKK and Schisandrin A is shown in Figure (7e), the interaction of TNF and Schisandrol B is shown in Figure (7f). Ertiprotafib with schisandrin A, satalanib with schisandrol B, fostamatinib with schisandrol B, copanlisib with schisandrol A. All the scores were comparable to those of the protein targets and positive drugs, suggesting that schisandrol A, schisandrin A, and schisandrol B may be the key active ingredients in SSAE in the treatment of ALD. The results are shown in Table 2 and Figure (7g).

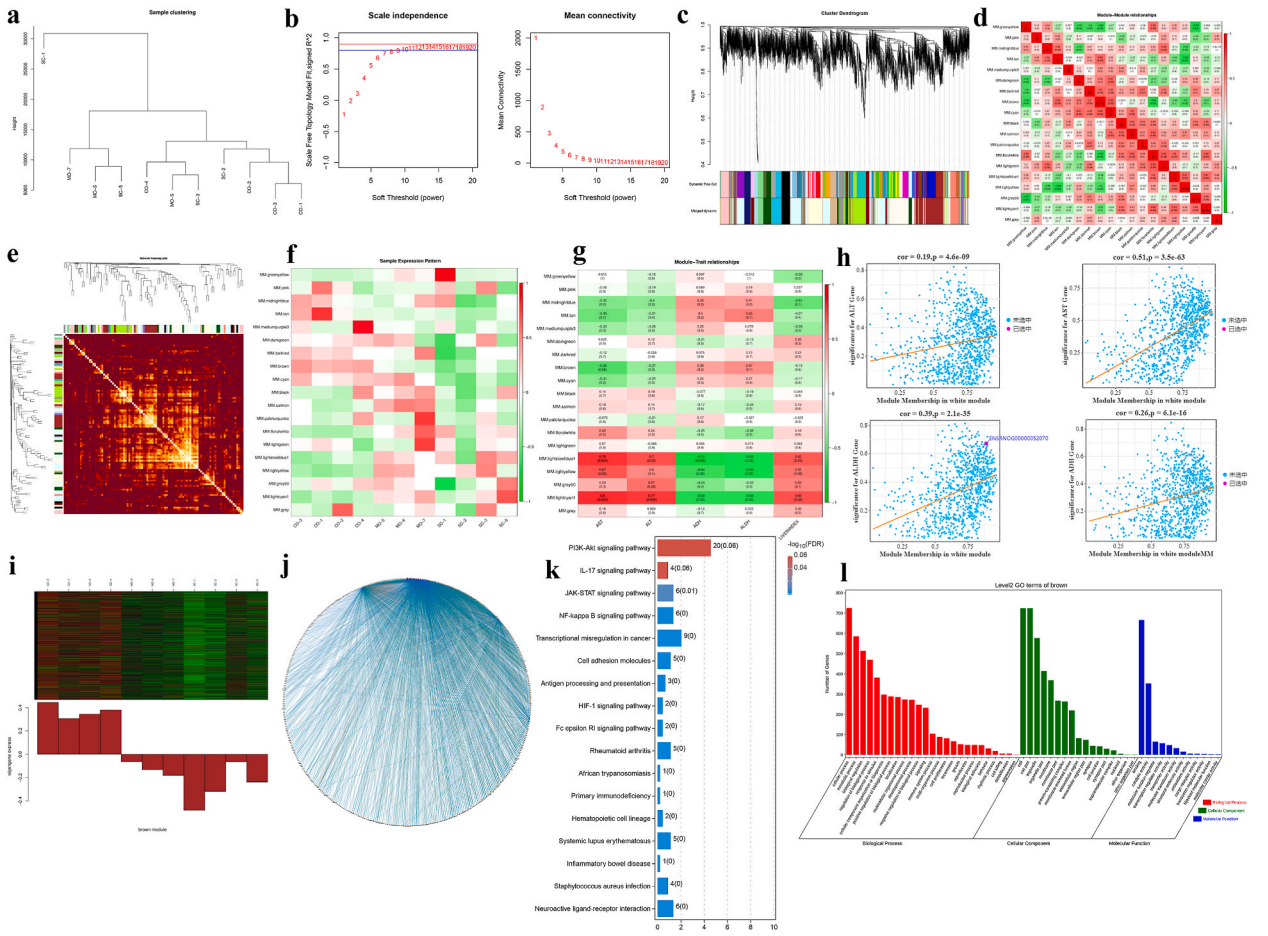

Fig. 5. Graph of WGCNA analysis results.
Note: The results of the hierarchical clustering of all sample as shown in (a); The connectivity of different modules as illustrated in (b); The results of 13 modules are shown in (c); The correlation results between two modules are shown in (d); The correlation analysis between gene expression and module eigenvalues is shown in (e); The correlation results of gene expression in key modules across different samples is shown in (f). The results of data correlation between module eigenvalues and specific traits and phenotypes are shown in (g); Pearson correlation results between each gene and trait data under the key module are presented in (h); The expression of genes in the key module across different samples is shown in (i); The gene co-expression network in the key module is visualized in (j); KEGG enrichment analysis of key module are shown in (k); GO enrichment analysis results as displayed in (l).

3.6. Quality control analysis results

3.6.1. High performance liquid chromatography analysis results

The results of the chromatogram of mixed control and the SSAE are shown in Figure (8a) and Figure (8b). The gradient elution procedure of HPLC is shown in Table 3.

3.6.2. Linearity analysis

For the linearity analysis, each high-concentration control solution was precisely pipetted into a 10 mL volumetric flask. Methanol was added to reach the mark, The solution was thoroughly mixed to obtain a mixed control and subjected to stepwise dilution to obtain solutions with concentrations of approximately 0.5 mg/mL, 0.1 mg/mL, 0.05 mg/mL, 0.01 mg/mL, 0.005 mg/mL, and 0.001 mg/mL. The peak areas of these solutions were recorded. A standard curve was constructed using the concentration as the X-axis and the peak area as the Y-axis. The lowest concentration point on the standard curve was used to further dilute the control solution in a stepwise manner. The regression reference equation is provided in Table 4.

3.6.3. Sample content determination

The samples to be analyzed were collected and assessed following the method described in section 2.8 The contents of schisandrol A, schisandrol B, and schisanin A were calculated based on the obtained results and are presented in Table 5.

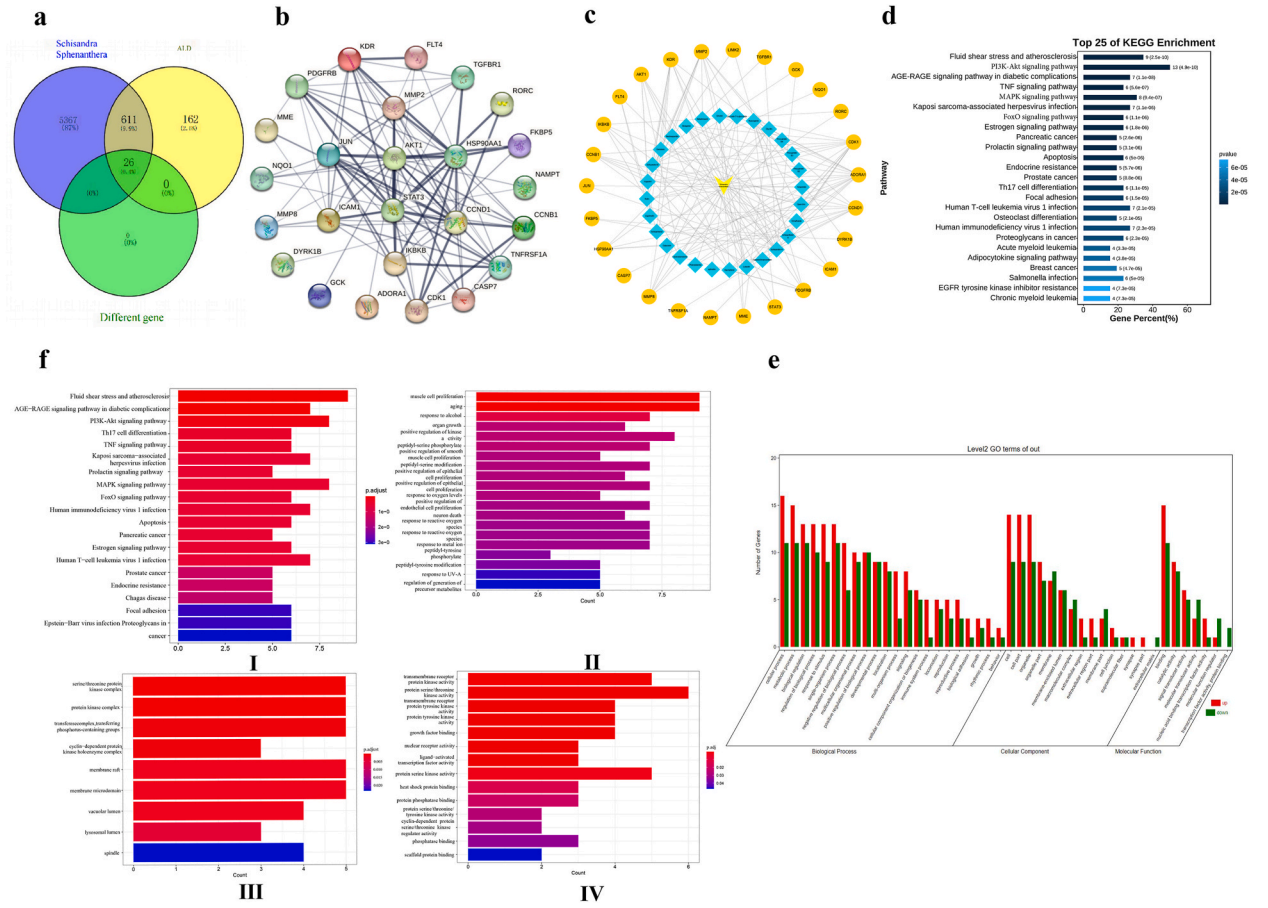

Fig. 6. Network construction and analysis and results as well as the outcomes of GO function and KEGG pathway enrichment analyses.
Note: (a) Map of intersecting gene targets, (b) PPI network map of key targets, (c) Cytoscape network map, (d) KEGG enrichment analysis, (e) GO enrichment analysis, (f) KEGG enrichment results and G0-enrichment results (BP.MF.CC). Note: Figure (f)-(I) is KEGG enrichment results, (II, III, IV) are G0-(BP, MF, CC) enrichment results.

3.7. Effects of different doses of SSAE on serum AST, ALT, ALDH, and ADH levels, liver index, and HE staining results in rats with ALD

The levels of AST, ALT, ALDH, and ADH in the serum were measured using ELISA kits. Compared to those in the control group, the results indicated a significant increase in the serum levels of AST, ALT ($p < 0.01$) and a significant decrease in the serum levels of ADH and ALDH ($p < 0.01$) in the model group in Figure (9b-9e). Additionally, the liver index was significantly elevated ($p < 0.01$) in the model group in Figure (9a). Compared to those in the model group, the ALT and AST contents, and liver index in the serum of the positive drug group and the SSAE high and middle dose groups were reduced ($p < 0.05$), whereas those of ADH and ALDH were increased ($p < 0.05$).

The results of HE staining showed that the overall structure of liver tissue in control rats appeared essentially normal, with hepatocytes exhibiting a well-preserved structure. No evident deformations such as hepatocyte edema and necrosis were observed. The liver sinusoids were radially arranged along the central vein, indicated by the black arrow, and no significant inflammatory cell infiltration was observed in the tissue in Figure (10a). In the model group, the liver tissue exhibited mild abnormalities in its overall structure, with a loosely arranged hepatocyte structure and hepatocyte edema, as shown by the black arrow in Figure (10b). The hepatic sinusoids were radially arranged along the central vein, the purple arrow indicates the hepatic sinusoidal macrophages, and the tissue exhibited obvious inflammatory cell infiltration. Compared to that in the model group, the liver tissue in the positive drug group displayed a mostly normal overall structure, with fuller hepatocytes, reduced hepatocyte edema, and decreased consolidation necrosisin in Figure (10c). Additionally, inflammatory cell infiltration was not significant. Furthermore, the low, middle, and high dose groups of SSAE exhibited reduced lesion severity are shown in Figure(10d-10f). Particularly, the liver tissue in the SSAE high and middle dose groups appeared mostly normal and exhibited fuller hepatocytes, reduced hepatocyte edema, and reduced consolidation necrosis, no significant inflammatory cell infiltration was observed in any of the tissues.

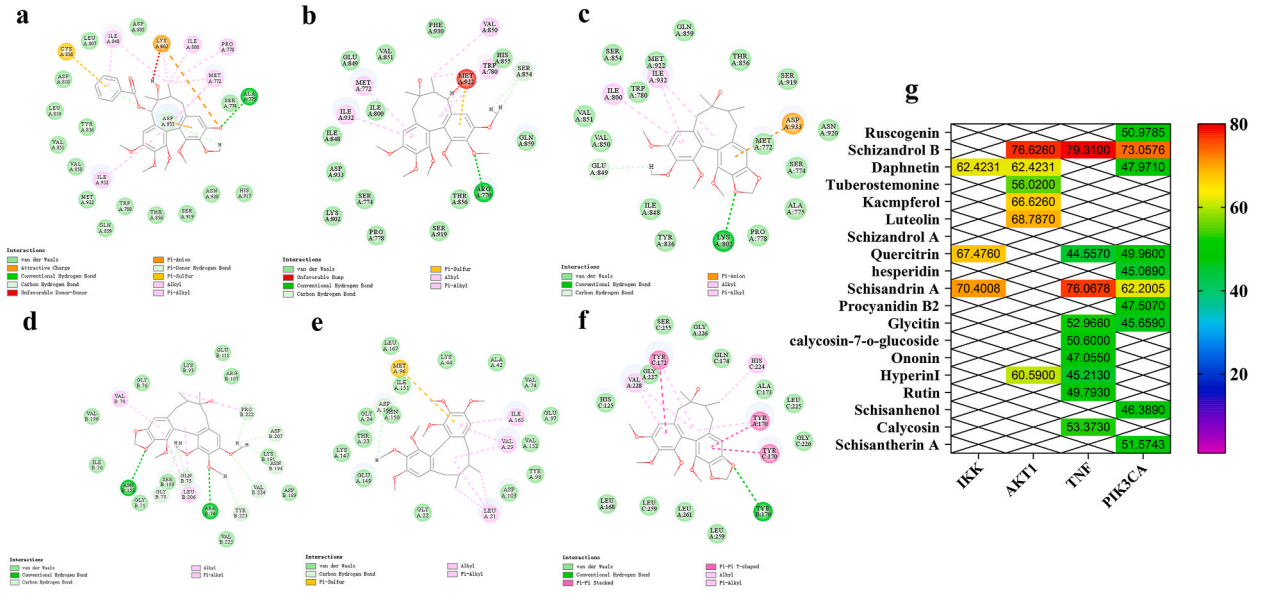

Fig. 7. Docking results for the key target proteins and their corresponding compound.
Note: (a) PIK3CA and Schisandrin A interaction diagram; (b) PIK3CA and Schisandrol A interaction diagram; (c) PIK3CA and Schiandrol B interaction diagram; (d) AKT1 and Schisandrol B interaction diagram; (e) IKK and Schisandrin A interaction diagram; (f) TNF and Schisandrol B interaction diagram; (g) Heat map of molecular docking.

Table 2
Fractions after docking target proteins with their corresponding compounds and positive drugs.

Key Targets	Components	Docking Score	Positive drugs	Docking Score
PIK3CA	Schisandrin A	51.5743	Copanlisib	72.2562
	Schisandrol A	62.2005		
	Schisandrol B	73.0576		
AKT1	Schisandrol B	76.626	Vatalanib	94.7767
IKK	Schisanthrin A	70.4008	Ertiprotafib	71.0992
TNF	Schisandrol B	79.31	Fostamatinib	78.86

3.8. Effect of different doses of SSAE on PI3K, p-PI3K, AKT, p-AKT, IKKα, p-IKKα, NFκB, p-NFκB and FOXO1 protein expression in the liver (Western Blotting analysis)

The results of Western Blotting imprinting are shown in Figure (11a,11b) and Figure (S1-S11). No difference in the protein expression levels of PI3K, AKT, IKKα, and NFκB was observed between the model group and the control group are shown in Figure (11d) and Figure (S6, S1, S3 and S8). However, the expression levels of p-PI3K, p-AKT, p-IKKα, and p-NFκB proteins were higher in the model group ($p < 0.005$), and the protein expression levels of FOXO1 were also significantly increased in the model group ($p < 0.005$) are shown in Figure (11c,**11i)** and Figure (S7, S2, S4, S9 and S10). In addition, p-PI3K/PI3K, p-AKT/AKT, p-IKKα/IKKα and p-NFκB/NFκB protein ratios were also significantly increased ($p < 0.01$) are shown in Figure(11e-11h). However, after oral administration of SSAE, the protein expression levels of p-AKT, p-IKKα, p-IKKα, and p-NFκB as well as p-PI3K/PI3K, p-AKT/AKT, p-IKKα/IKKα, and p-NFκB/NFκB protein ratios were significantly reduced in the middle-dose and high-dose groups, compared to those in the model group ($p < 0.05$) are shown in Figure(11c,**11e-11h)**. Moreover, the expression level of FOXO1 protein was also significantly reduced ($p < 0.01$) is shown in Figure(11i) and Fig. S10. Compared with the model group, there was a significant difference between medium and high doses of SSAE ($p < 0.01$). These results indicated that SSAE could target and regulate the PI3K-AKT signaling pathway, attenuate the inflammatory injury and apoptosis in liver tissues, and achieve the improvement and treatment of ALD.

3.9. Immunohistochemical detection of the protein expression of p-AKT, p-IKKα, and Bcl-2 in liver tissues

The expression levels of p-AKT, p-Ikkα, and Bcl-2 in rat liver tissues were measured by immunohistochemical assay. The results of immunohistochemistry is shown in Figure (12a) and the immunopositive cells showed different degrees of yellow-brown color. Compared with those in the control groups the expression levels of p-AKT and p-IKKα were significantly higher ($p < 0.01$) and Bcl-2 were significantly lower ($p < 0.01$) in the model group are shown in Figure (12b-12d). Compared with those in the model group, the protein expression levels of p-AKT and p-IKKα in group of positive drugs, the SSAE high dose group and the middle-dose group were

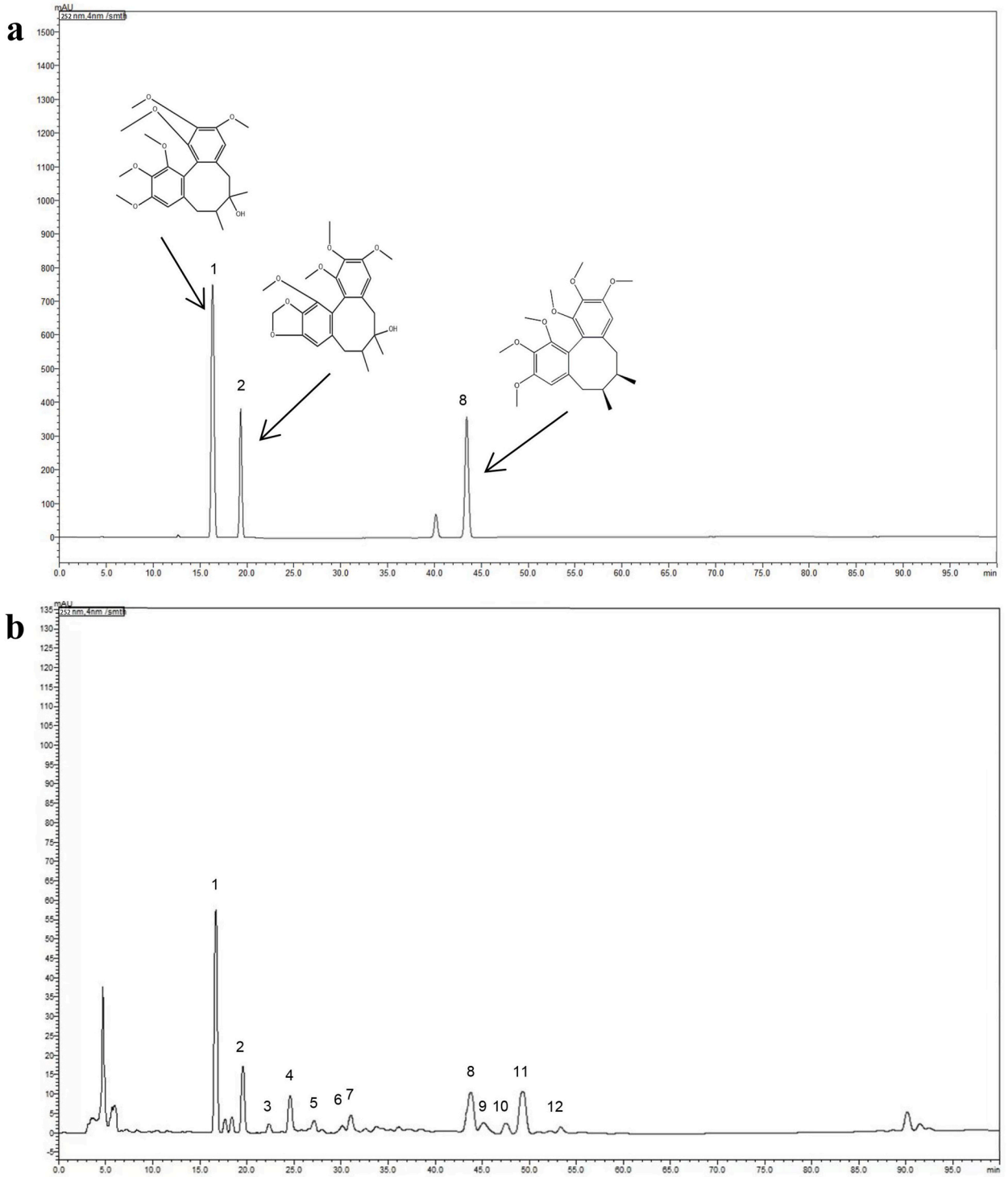

Fig. 8. (a) Mixed control. (b) SSAE chromatogram.
Note: (No.1 Schisandrol A; No.2 Schisandrol B; No.8 Schisandrin A).

reduced to different degrees ($p < 0.05$), whereas the expression levels of Bcl-2 protein were significantly increased ($p < 0.05$). The results indicated that SSAE could reduce the protein expression of p-AKT and p-IKKα in the liver of rats with ALD. Moreover, the expression of Bcl-2 in the liver was increased, ultimately achieving the therapeutic effect in ALD.

Table 3
Gradient elution procedure.

No	time/min	acetonitrile (%)	Water (%)
1	0	45	55
2	20	45	55
3	30	60	40
4	40	65	35
5	60	65	35
6	70	75	25
7	80	85	15
8	90	95	5
9	100	100	0

Table 4
Reference regression equation and linear range.

Reference substance	Regression equation	R^2	Linear Range(mg/ml)
Schisandrol A	y = 7E+06x-322851	0.9995	0.00124–6.2
Schisandrol B	y = 3E+06x-108355	0.9997	0.00112–5.6
Schisanthrin A	y = 4E+06x-137357	0.9997	0.00114–5.7

Table 5
Content determination results.

Components	Content(mg/ml)
Schisandrol A	0.30925
Schisandrol B	0.27661
Schisanthrin A	0.22714

4. Discussion

ALD is a growing clinical concern and has emerged as a significant cause of liver disease, following viral hepatitis [30]. Oxidative stress damage and impaired alcohol-induced free radical scavenging activity have been identified as key factors contributing to ALD [30,31]. Elevated levels of AST and ALT are commonly observed pathological and serological features [32–34]. Severe cases of ALD are characterized by liver cell apoptosis. In this study, ALD was induced in rats by oral administration of white spirit, and the rats in the model group were treated with SSAE. The serum levels of AST and ALT were significantly elevated, the levels of ADH and ALDH were significantly decreased, and the liver indices were significantly elevated. Moreover, histopathological examination showed a large infiltration of inflammatory cells in the liver of the rats with ALD and abnormalities in the trait structure of liver cells. These finding are consistent with the results of several studies. Moreover, the phosphorylation levels of AKT and IKK proteins in liver tissue cells of rats were significantly increased in the model group, suggesting successful modeling of ALD rats. Notably, SSAE reversed this effect, suggesting that SSAE may play a certain therapeutic role in ALD, and also providing a preliminary basis for our subsequent study.

Transcriptome sequencing, WGCNA and GO functional enrichment analysis of ALD DEGs by joint network pharmacology showed that SSAE is regulated through cellular process, metabolic process, biological regulation, positive regulation of the biological process, catalytic activity, transporter activity, antioxidant activity, cell part, protein-containing complex, cell junction, and other processes. The KEGG pathway enrichment analysis showed that SSAE alleviates ALD by acting on PI3K/AKT and NFκB pathways, The PI3K/AKT signaling pathway can regulate the release of inflammatory factors and the formation of enzymes related to proliferation, inflammation, and apoptosis, and participates in the pathology of ALD. The PI3K/AKT/IKK signaling pathway is widely present and in an upregulated state of expression in abnormal hepatocytes [35], PI3K/AKT/IKK phosphorylation activates IL-1β and induces overexpression of pro-inflammatory factors TNF-α and IL-6, mediating the development of liver inflammation in rats [36]. IKK activates the phosphorylation of IκB and the subsequent nuclear translocation of NFκB, increases the level of inflammatory mediators, may underly the immune defense and immune regulation in ALD [37–39]. Furthermore, the overexpression of numerous pro-inflammatory factors exacerbates the inflammatory response, leading to hepatocyte necrosis and cellular dysregulation [40]. AKT, through phosphorylation activation or inhibition, regulates cell survival by regulating proteins such as cystathione-aspase Caspase, Bcl-2 and FOXO1 [19,41]. The anti-apoptotic gene Bcl-2 is particularly significant in the regulation of normal liver function and hepatocellular carcinoma [42]. Inhibition of the aberrantly activated PI3K/AKT/IKK and NFκB pathway further reduces the inflammatory response and regulates the Bcl-2 and FOXO1 protein, which has a therapeutic effect on ALD. Therefore, the mechanism of action of SSAE for ALD treatment may involve inflammatory apoptosis-related pathways. Based on the above results, molecular docking was performed in the present study to assess the interaction between the active components of SSAE and key targets, including IKK, AKT1, TNF, and PIK3CA on the PI3K/AKT pathway. The results indicated stable binding between the active components and the key targets, in which schisandrol A, schisandrol B and schisandrin A generally scored higher than the other components with the key targets, These finding suggest the

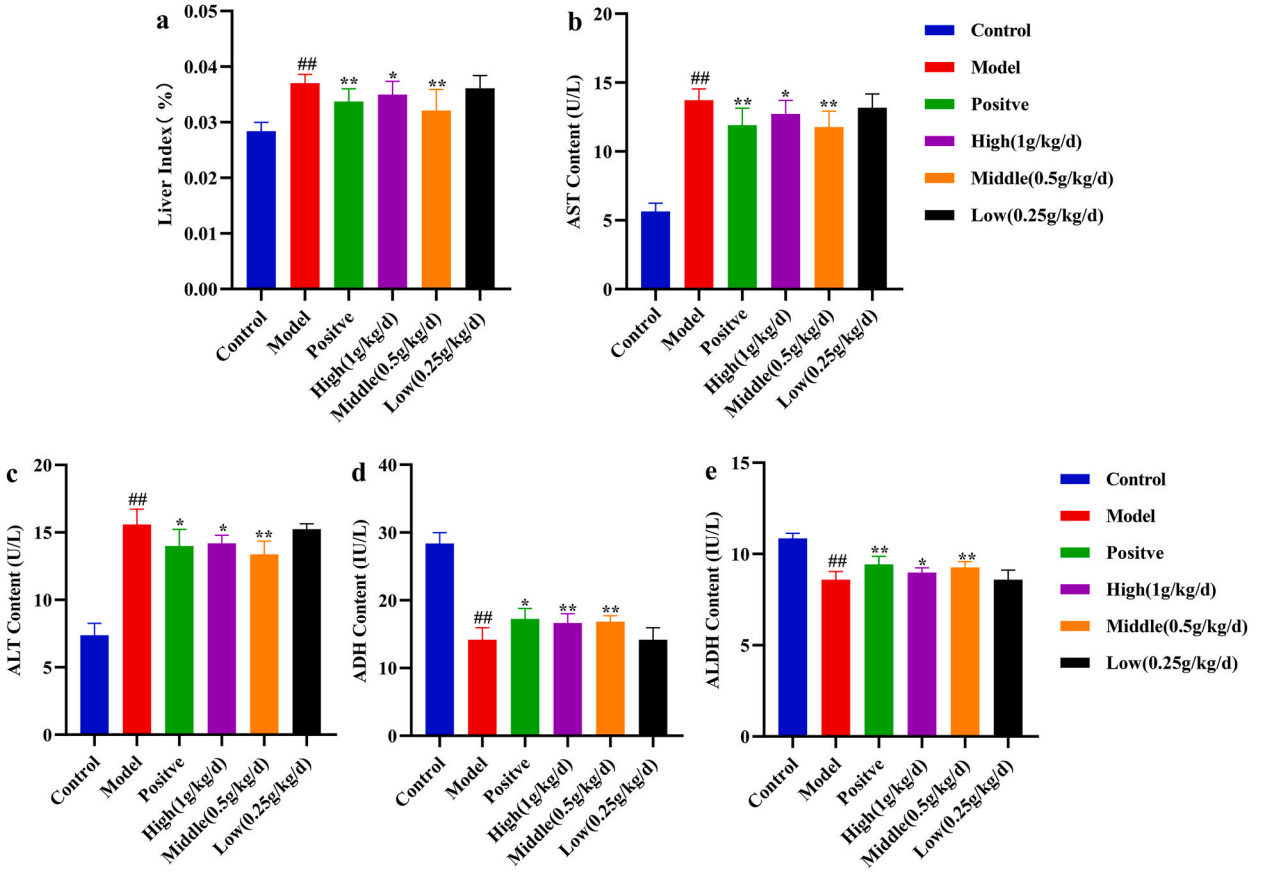

Fig. 9. (a) Depicts liver index measurements. (b, c, d, e) The results of AST, ALT, ADH, and ALDH kits, respectively. ($^{\#}p < 0.05$, $^{*}p < 0.05$).

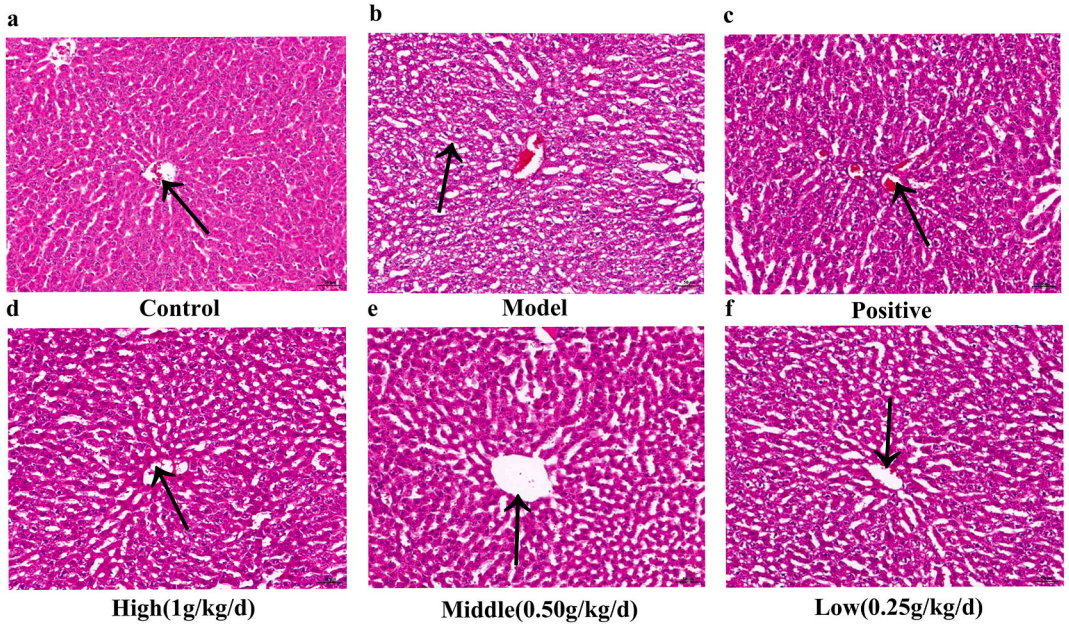

Fig. 10. SSAE on the histopathological morphology of rat liver (HE, × 200).
Note: (a) Control (b) Model (c) Positive (d) High (e) Middle (f) Low.

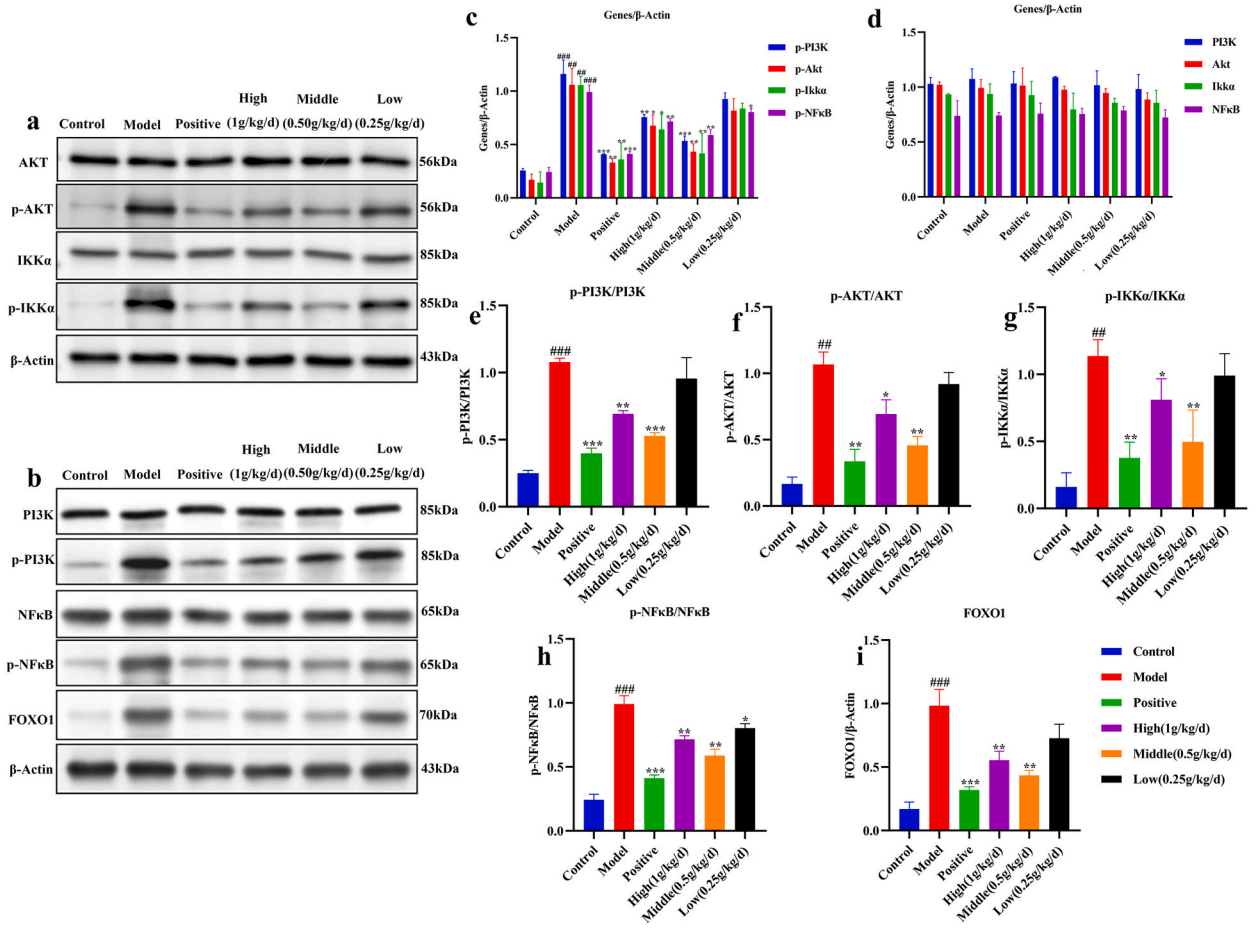

Fig. 11. Trend of Protein expression of PI3K, AKT, IKKα, NFκB and FOXO1 in the liver tissues of rats in each group.
Note: (a, b) Protein blots of PI3K, p-PI3K, AKT, p-AKT, IKKα, p-IKKα, NFκB, p-NFκB, FOXO1. The non-adjusted, full images for Western blotting are shown in Figure (S1–S11); (c) Quantitative analysis of p-PI3K, p-AKT, p-IKKα, p-NFκB; (d) Quantitative analysis of PI3K, AKT, IKKα, NFκB; (e) Ratio of p-PI3K to PI3K; (f) Ratio of p-AKT to AKT; (g) Ratio of p-IKKα to IKKα; (h) Ratio of p- NFκB to NFκB; (i) Quantitative analysis of FOXO1; (**$^{\#}p < 0.05$, $^{*}p < 0.05$**).

importance of these three compounds as key compounds for SSAE in the treatment of ALD. Studies have shown that schisandrin A exerts anti-inflammatory effects in cells, inhibits ROS production, reduces TNF activity, and blocks the phosphorylation of IKKα and IκB and the subsequent nuclear translocation of NFκB, leading to NFκB inhibition [43]. Moreover, IκBα is a key protein in the NFκB pathway and is required for NFκB activation. It is also a major regulatory inhibitory protein of NFκB (p50-p65). schisandrol A significantly reduces intracellular reactive oxygen species accumulation by inhibiting NFκB, and PI3K/AKT pathways, conferring a protective effect on inflammatory and oxidative responses in cells [43–45]. Schisandrol B can mediate the activation of AKT and modulate IκB kinase thereby ameliorating oxidative damage in rat hepatocytes. These findings highlight their critical role as active ingredients in ALD treatment. Therefore, under pathological conditions, activation of IκB kinase by inhibition of AKT phosphorylation, which in turn inhibits degradation of IκB (IκB is an inhibitor of NFκB), prevents translocation of the transcription factor NFκB to the nucleus, and inhibits up-regulation of genes in the PI3K/AKT signalling pathway, ultimately attenuating inflammation and the cellular regulatory response [42]. Our study revealed that SSAE may exerts its therapeutic effect on ALD by downregulating PI3K, AKT, IKK and NFκB phosphorylation levels and the protein expression of FOXO1 and upregulating the expression of Bcl-2 protein. The mechanism of action is shown in Figure (13).

In this study, the active chemical components of SSAE were comprehensively and accurately identified through UPLC-Q-TOF-MS/MS analysis. This analytical approach establishes a strong foundation for further exploration and analysis of the pharmacological substances present in SSAE. Moreover, RNA-seq, WGCNA analysis network pharmacology, and animal experiments are used to further explore the mechanism of action of ALD. These findings offer a significant theoretical basis for the future development and utilization of traditional Chinese medicine as related health and functional foods in the treatment of ALD.

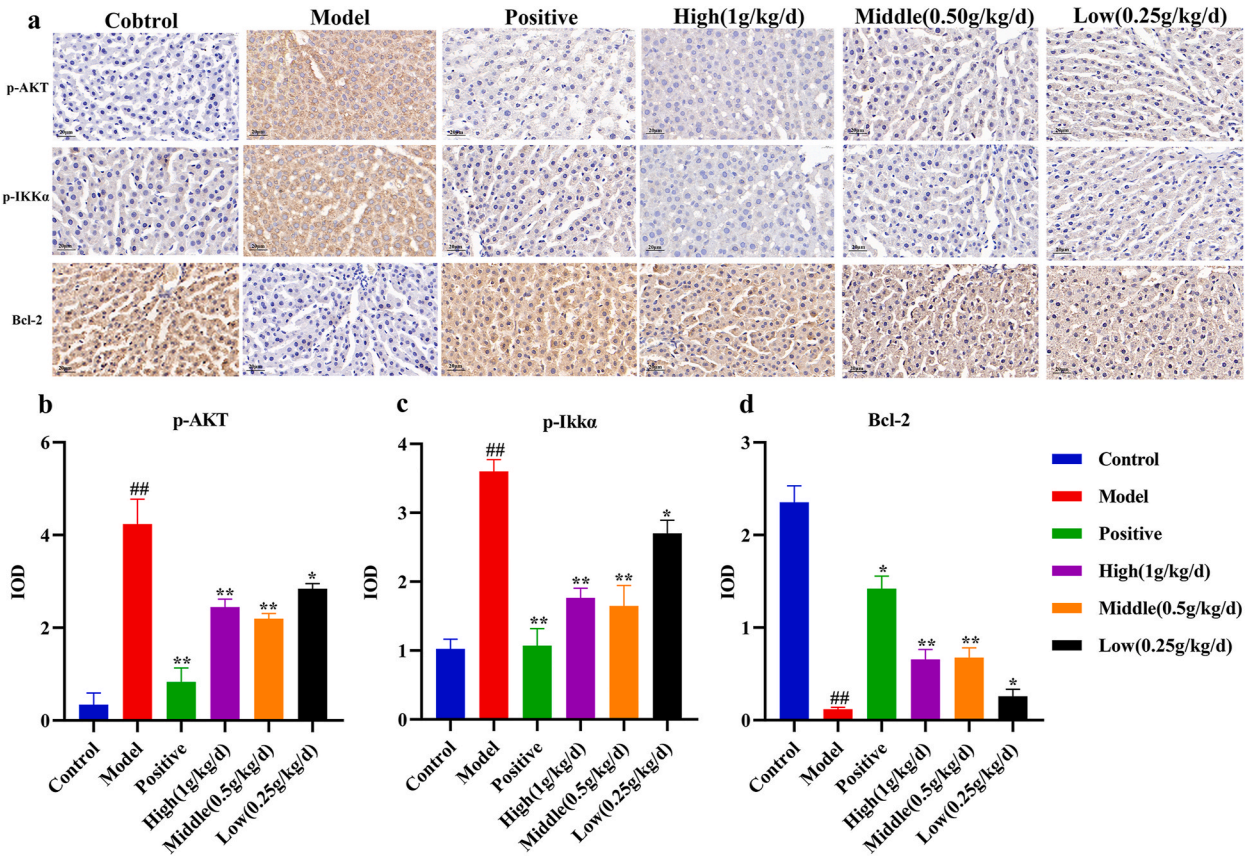

Fig. 12. Immunohistochemical results.
Note: (a) The results of immunohistochemistry, and (b, c, d) the results of positive expression trends of p-AKT, p-IKKα, and Bcl-2 proteins in the liver tissues of rats in each group(**$^{\#}p < 0.05$, $^{*}p < 0.05$**).

5. Conclusion

The results of this study demonstrate the efficacy of SSAE in treating ALD rats. The chemical composition of SSAE was analyzed and identified by UPLC-Q-TOF-MS/MS, and the serum levels of ALDH, ADH, AST, and ALT were measured by ELISA and biochemical kits. The protein phosphorylation status of PI3K, AKT, IKK and NFκB and the protein expression level of FOXO1 were assessed by Western blotting analysis. Immunohistochemistry was used to determine the positive expression of p-AKT, p-IKK, and Bcl-2 in each group of rats. It was further hypothesized that the core components of SSAE, such as schisandrol A, schisandrol B, and schisandrin B, may downregulate PI3K, AKT, IKK, NFκB phosphorylation levels, and the protein expression of FOXO1 and upregulated the protein expression of Bcl-2 protein. These findings suggest that SSAE may exert protective effects on ALD partly through PI3K/AKT/IKK signaling pathway. This study provide reference for future research and treatment of ALD and the development of novel natural liver-protective foods. However, the present study did not systematically and comprehensively investigate and validate the effect of SSAE in the treatment of ALD as a result of multiple pathways and multiple inhibitory interactions. This aspect should be addressed in future research endeavors.

Funding

This project was supported by the National Key R&D Program (2021YFD1601004), Shaanxi Provincial Engineering Research Center for Traditional Chinese Medicine, Shaanxi Provincial Administration of Traditional Chinese Medicine “Qin Medicine” Development Key Research Project (2021-02-22-014), the Project of Shaanxi Provincial Department of Science and Technology(2022JM-555), the Project of Shaanxi Provincial Department of Science and Technology(2023-YBSF-474), Shaanxi University of Traditional Chinese Medicine University-level Project (2021GP29), the Key R&D Programme of Xianyang City (L2023-ZDYF-SF-019), the Project of Xi’an Municipal Bureau of Science and Technology (2023JH-JSJQ-0007) and the Project of Science and Technology Department of Inner Mongolia Autonomous Region.

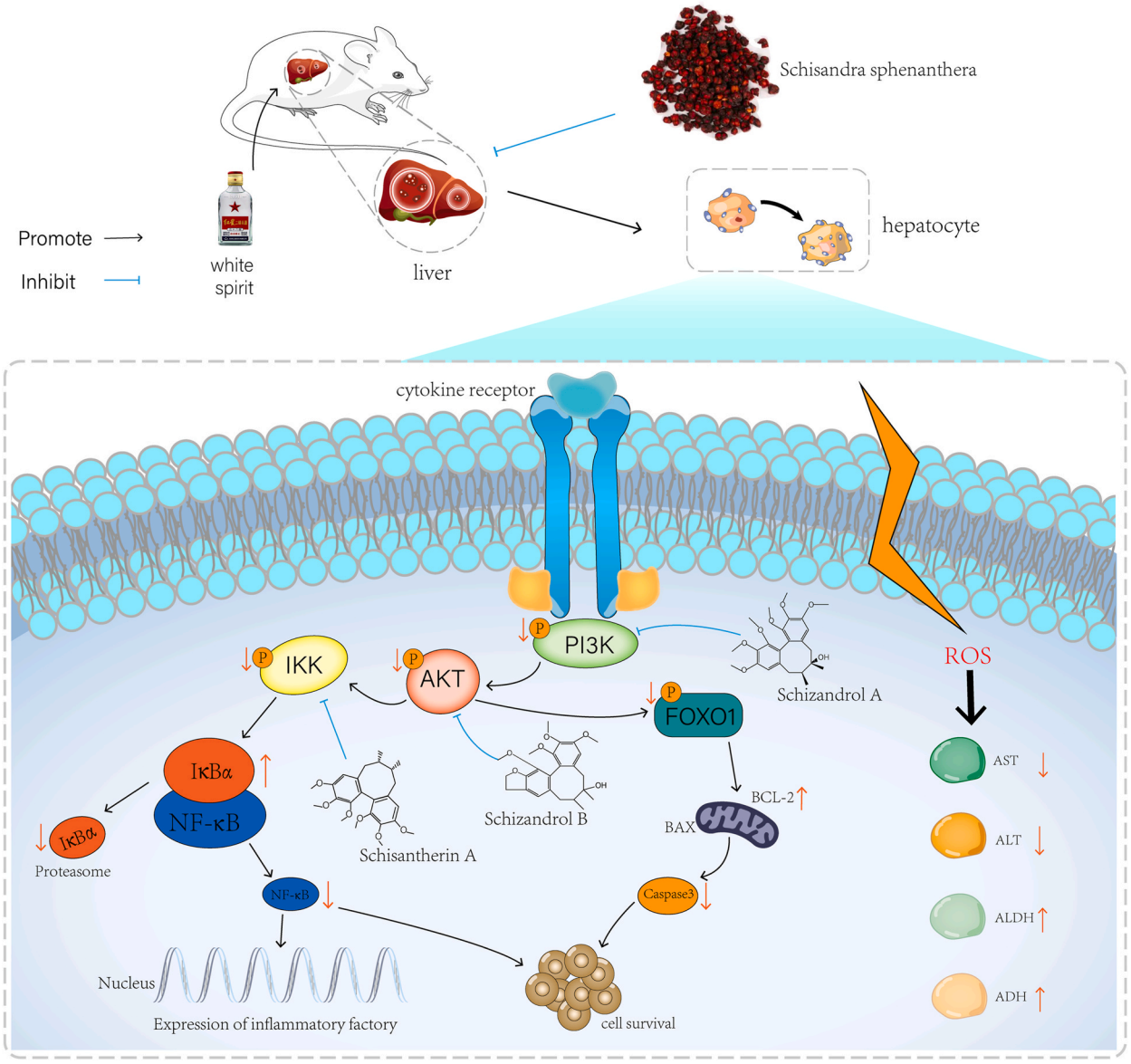

Fig. 13. Mechanism diagram.

Ethics statement

This study was approved by the Animal Ethics Committee of Shaanxi University of Traditional Chinese Medicine for the humane care of animals (approval number SUCMDC20220530002).

Data availability

The data presented in the study are deposited in the SRA databage repository, accesgion number PRJNA981095.

CRediT authorship contribution statement

Ding Liu: Writing – original draft, Conceptualization. **Kai Yang:** Writing – original draft, Conceptualization. **Taotao Li:** Software, Methodology. **Tiantian Tang:** Software, Methodology. **Yujiao Wang:** Software, Methodology. **Wenfei Wang:** Software, Methodology. **Jia Li:** Software, Methodology. **Peijie Zhou:** Validation, Investigation, Formal analysis. **Xuan Wang:** Validation, Investigation, Formal analysis. **Chongbo Zhao:** Validation, Investigation, Formal analysis. **Dongyan Guo:** Validation, Investigation, Formal analysis. **Yundong Xie:** Validation, Investigation, Formal analysis. **Jiangxue Cheng:** Data curation. **Mei Wang:** Data curation. **Jing Sun:**

Writing – original draft, Funding acquisition. **Xiaofei Zhang:** Writing – original draft, Funding acquisition.

Declaration of competing interest

The authors declare that they have no known competing financial interests or personal relationships that could have appeared to influence the work reported in this paper.

Appendix A. Supplementary data

Supplementary data to this article can be found online at https://doi.org/10.1016/j.heliyon.2024.e34214.

References

[1] M. Hartleb, E. Czech, Alcoholic liver disease (ALD), Przeglad Gastroenterologiczny 2 (2) (2007) 92–100.
[2] B. Gao, Hepatoprotective and anti-inflammatory cytokines in alcoholic liver disease, J. Gastroenterol. Hepatol. 27 (2012) 89–93, https://doi.org/10.1111/j.1440-1746.2011.07003.x.
[3] H. Seitz, R. Bataller, H. Cortez-Pinto, et al., Alcoholic liver disease, Nat. Rev. Dis. Prim. (2018) 4, https://doi.org/10.1038/s41572-018-0014-7.
[4] L. Shan, Z. Liu, L. Ci, et al., Research progress on the anti-hepatic fibrosis action and mechanism of natural products, Int. Immunopharm. (2019) 75, https://doi.org/10.1016/j.intimp.2019.105765.
[5] P. Zhu, J. Li, X. Fu, et al., Schisandra fruits for the management of drug-induced liver injury in China, Phytomedicine 59 (2019), https://doi.org/10.1016/j.phymed.2018.11.020.
[6] Y. Wang, Z. Qiu, Y. Gao, et al., Application of Fructus Schisandrae chinensis in health food, Asia-Pacific Traditional Medicine 19 (1) (2023) 216–219, https://doi.org/10.11954/ytctyy.202301050.
[7] H. Liu, H. Lai, X. Jia, et al., Comprehensive chemical analysis of Schisandra chinensis by HPLC–DAD–MS combined with chemometrics, Phytomedicine 20 (12) (2013) 1135–1143, https://doi.org/10.1016/j.phymed.2013.05.001.
[8] A. Szopa, R. Ekiert, H. Ekiert, Current knowledge of Schisandra chinensis (Turcz.) Baill. (Chinese magnolia vine) as a medicinal plant species: a review on the bioactive components, pharmacological properties, analytical and biotechnological studies, Phytochemistry, Review 16 (2) (2017) 195–218, https://doi.org/10.1007/s11101-016-9470-4.
[9] Y. Lu, D. Chen, Analysis of Schisandra chinensis and Schisandra sphenanthera, J. Chromatogr. 1216 (11) (2009) 1980–1990, https://doi.org/10.1016/j.chroma.2008.09.070.
[10] M. Hong, Y. Zhang, S. Li, et al., A network pharmacology-based study on the hepatoprotective effect of Fructus Schisandrae, Molecules 22 (2017) 1617, https://doi.org/10.3390/molecules22101617.
[11] P. Zhu, J. Li, X. Fu, et al., Schisandra fruits for the management of drug-induced liver injury in China, Phytomedicine 59 (2019) 152760, https://doi.org/10.1016/j.phymed.2018.11.020.
[12] K. Yang, J. Qiu, Z. Huang, et al., A comprehensive review of ethnopharmacology, phytochemistry, pharmacology, and pharmacokinetics of Schisandra chinensis (Turcz.) Baill. and Schisandra sphenanthera Rehd. et Wils, J. Ethnopharmacol. 284 (2022), https://doi.org/10.1016/j.jep.2021.114759.
[13] Z. Chen, F. Liu, N. Zheng, et al., Wuzhi capsule (Schisandra Sphenanthera extract) attenuates liver steatosis and inflammation during non-alcoholic fatty liver disease development, Biomed. Pharmacother. 110 (2019) 285–293, https://doi.org/10.1016/j.biopha.2018.11.069.
[14] Y. Gao, S. Wu, R. Cong, et al., Characterization of lignans in Schisandra chinensis oil with a single analysis process by UPLC-Q/TOF-MS, Chem. Phys. Lipids 218 (2019) 158, https://doi.org/10.1016/j.chemphyslip.2018.12.012, 16.
[15] H. Shen, Y. Zhou, J. Zheng, et al., Mechanism of action of "multi-component-multi-target-multi-pathway" based on network pharmacology of Sunflower Liver Tablets, China Journal of Chinese Medicine 44 (7) (2019) 1464–1474, https://doi.org/10.19540/j.cnki.cjcmm.20181214.003.
[16] Y. Wang, Observation on the efficacy of Sunflower Liver Protecting Tablets in the treatment of drug-induced liver injury, Pharmacoeconomics of China 13 (11) (2018) 79–81, https://doi.org/10.12010/j.issn.1673-5846.2018.11.016.
[17] M. Wu, Sunflower liver protection Tablets for the prevention of liver damage caused by Hypertension in the treatment of Telmisartan Tablets, China Prescription Drugs 15 (8) (2017) 69.
[18] N. Zhang, H. Yang, X. Yan, et al., Hepatic metabolomics of Hovenia dulcis in the prevention of alcoholic liver injury in rats, J. Shenyang Pharm. Univ. 37 (11) (2020) 1003–1008, https://doi.org/10.14066/j.cnki.cn21-1349/r.2020.11.007.
[19] Y. Jiang, M. Zhong, H. Zhan, et al., Integrated strategy of network pharmacology, molecular docking, HPLC-DAD and mice model for exploring active ingredients and pharmacological mechanisms of Penthorum chinense Pursh against alcoholic liver injury, J. Ethnopharmacol. 298 (2022) 115589, https://doi.org/10.1016/j.jep.2022.115589.
[20] L. Su, P. Li, T. Lu, et al., Protective effect of Schisandra chinensis total lignans on acute alcoholic-induced liver injury related to inhibiting CYP2E1 activation and activating the Nrf2/ARE signaling pathway, Revista Brasileira de Farmacognosia 29 (2) (2019) 198–205, https://doi.org/10.1016/j.bjp.2019.01.008.
[21] H. Zhu, W. Jiang, C. Liu, et al., Ameliorative effects of chlorogenic acid on alcoholic liver injury in mice via gut microbiota informatics, Eur. J. Pharmacol. 928 (2022) 175096, https://doi.org/10.1016/j.ejphar.2022.175096.
[22] J. Shao, J. Zhang, H. Guo, et al., Clinical application of Schisandra chinensis and its dosage, Medicine in Jilin. China 39 (2) (2019) 162–164+168, https://doi.org/10.13463/j.cnki.jlzyy.2019.02.007.
[23] S. Liu, N. Mancipe, T. Gisslen, et al., Identification of genes responding to iron or choline treatment for early-life iron deficiency in the male rat hippocampal transcriptomes, J. Nutr. (2024), https://doi.org/10.1016/j.tjnut.2024.02.021.
[24] Y. Wang, X. Wang, T. Tang, et al., Basis with RNA-Seq and WGCNA to explore the effect of Frankincense essential oil on dextran sodium sulfate-induced ulcerative colitis through MAPK/NF-κB signaling, Fitoterapia 172 (2024) 105744, https://doi.org/10.1016/j.fitote.2023.105744.
[25] J. Li, J. Duan, Y. Wang, et al., The JAK/STAT/NF-κB signaling pathway can be regulated by rosemary essential oil, thereby providing a potential treatment for DNCB-induced in mice, Biomed. Pharmacother. 168 (2023) 115727, https://doi.org/10.1016/j.biopha.2023.115727.
[26] X. Wang, P. Zhou, H. Shi, et al., Cinnamon essential oil based on NLRP3 inflammasome and renal uric acid transporters for hyperuricemia, Food Biosci. 56 (2023) 103285, https://doi.org/10.1016/j.fbio.2023.103285.
[27] T. Li, W. Wang, Q. Guo, et al., Rosemary (Rosmarinus officinalis L.) hydrosol based on serotonergic synapse for insomnia, J. Ethnopharmacol. 318 (2024) 116984, https://doi.org/10.1016/j.jep.2023.116984.
[28] J. Duan, J. Li, Y. Wang, et al., Therapeutic effects and mechanism of action of lavender essential oil on atopic dermatitis by modulating the STAT3/RORγt pathway, Arab. J. Chem. 17 (2) (2024) 105525, https://doi.org/10.1016/j.arabjc.2023.105525.
[29] S. Wang, H. Liang, J. Huang, et al., Simultaneous determination of seven lignans in Schisandra chinensis by HPLC, Modern Chinese Medicine, China 21 (4) (2019) 473–477, https://doi.org/10.13313/j.issn.1673-4890.20181016006.
[30] G. Arteel, Animal models of alcoholic liver disease, Dig. Dis. 28 (6) (2010) 729–736, https://doi.org/10.1159/000324280.
[31] W. Dunn, V. Shah, Pathogenesis of alcoholic liver disease, Clin. Liver Dis. 20 (3) (2016) 445, https://doi.org/10.1016/j.cld.2016.02.004.

[32] J. Li, X. Lu, P. Jia, et al., O-alkyl and o-benzyl hesperetin derivative-1L attenuates inflammation and protects against alcoholic liver injury via inhibition of BRD2-NF-kappa B signaling pathway, Toxicology 466 (2022), https://doi.org/10.1016/j.tox.2021.153087.
[33] J. Wang, X. Chen, P. Hu, et al., Effects of Linderae radix extracts on a rat model of alcoholic liver injury, Exp. Ther. Med. 11 (6) (2016) 2185–2192, https://doi.org/10.3892/etm.2016.3244.
[34] J. Qiao, H. Li, F. Liu, et al., Effects of portulaca oleracea extract on acute alcoholic liver injury of rats, Molecules 24 (16) (2019), https://doi.org/10.3390/molecules24162887.
[35] Z. Zhao, J. Gao, C. Li, et al., Reactive oxygen species induce endothelial differentiation of liver cancer Stem-like sphere cells through the activation of Akt/IKK signaling pathway, Oxid. Med. Cell. Longev. (2020) 1621687, https://doi.org/10.1155/2020/1621687.
[36] Y. Wu, S. Liu, T. Ren, et al., Ginseng fermentation solution affects the gut microbiota in zebrafish with Alcoholic liver disease via PI3K/Akt pathway, Phytomedicine (2024) 155495, https://doi.org/10.1016/j.phymed.2024.155495.
[37] S. Zhou, W. Zhao, J. Li, et al., Bioinformatics analysis identifies TNFRSF1A as a biomarker of liver injury in sepsis TNFRSF1A is a biomarker for septic liver injury, Genetics Research 2022 (2022) 1493744, https://doi.org/10.1155/2022/1493744.
[38] Y. Ma, Z. Zhu, Z. Peng, et al., Can "Fire" change medicinal effects? Processing heat transforms the efficacy of Chaihu from antipyretic to hepatic-soothing, Pharmacological Research - Modern Chinese Medicine 10 (2024) 100385, https://doi.org/10.1016/j.prmcm.2024.100385.
[39] Z. Peng, X. Gong, Y. Yang, et al., Hepatoprotective effect of quercetin against LPS/d-GalN induced acute liver injury in mice by inhibiting the IKK/NF-κB and MAPK signal pathways, Int. Immunopharm. 52 (2017) 281–289, https://doi.org/10.1016/j.intimp.2017.09.022.
[40] C. Ding, Y. Zhao, X. Chen, et al., Taxifolin, a novel food, attenuates acute alcohol-induced liver injury in mice through regulating the NF-κB-mediated inflammation and PI3K/Akt signalling pathways, Pharmaceut. Biol. 59 (1) (2021) 866–877, https://doi.org/10.1080/13880209.2021.1942504.
[41] Y. Zhao, X. Liu, C. Ding, et al., Dihydromyricetin reverses thioacetamide-induced liver fibrosis through inhibiting NF-κB-Mediated inflammation and TGF-β1-regulated of PI3K/Akt signaling pathway, Front. Pharmacol. 12 (2021), https://doi.org/10.3389/fphar.2021.783886.
[42] R. Jiang, J. Tang, X. Zhang, et al., CCN1 promotes inflammation by inducing IL-6 production via α6β1/PI3K/Akt/NF-κB pathway in autoimmune hepatitis, Front. Immunol. 13 (2022), https://doi.org/10.3389/fimmu.2022.810671.
[43] D. Kwon, H. Cha, E. Choi, et al., Schisandrin A suppresses lipopolysaccharide-induced inflammation and oxidative stress in RAW 264.7 macrophages by suppressing the NF-κB, MAPKs and PI3K/Akt pathways and activating Nrf2/HO-1 signaling, Int. J. Mol. Med. 41 (1) (2018) 264–274, https://doi.org/10.3892/ijmm.2017.3209.
[44] N. Arken, Schizandrol A reverses multidrug resistance in resistant chronic myeloid leukemia cells K562/A02, Cell. Mol. Biol. 65 (1) (2019) 78–83, https://doi.org/10.14715/cmb/2019.65.1.14.
[45] H. Xian, W. Feng, J. Zhang, Schizandrin A enhances the efficacy of gefitinib by suppressing IKKβ/NF-κB signaling in non-small cell lung cancer, Eur. J. Pharmacol. 855 (2019) 10–19, https://doi.org/10.1016/j.ejphar.2019.04.016.
[46] Z. Zhang, S. Li, Y. Zuo, UPLC-Q-TOF-MS/MS characterization and HPLC content determination of lime and sweet orange flowers, Central South Pharmacy 20 (11) (2022) 2480–2489, https://doi.org/10.7539/j.issn.1672-2981.2022.11.005.
[47] W. Xu, Z. Fu, J. Lin, et al., Qualitative and quantitative studies on the major components of Trifolium pratense by HPLC-Q-TOF-MS and UPLC-QqQ-MS, China Journal of Traditional Chinese Medicine 39 (22) (2014) 4365–4372, https://doi.org/10.4268/cjcmm20142218.
[48] G. Sun, J. Huo, W. Pan, et al., Chemical composition analysis of Sophora japonica herbs based on UPLC-Q-TOF/MS technique, Chinese herbal medicine 50 (16) (2019) 3774–3783, https://doi.org/10.7501/j.issn.0253-2670.2019.16.007.
[49] L. Lai, Y. Lin, F. Chen, et al., HPLC-Q-TOF-MS and HPLC-DAD based analysis of the main active components of G, kamenensis, Chinese herbal medicine 47 (20) (2016) 3578–3585, https://doi.org/10.7501/j.issn.0253-2670.2016.20.006.
[50] L. Zhong, F. Yang, J. Wu, et al., Prediction of quality markers for anticoagulant activity of Kunning granules based on UPLC-Q-TOF-MS/MS and spectroscopy, Chinese Journal of Experimental Formulas 29 (7) (2023) 168–176, https://doi.org/10.13422/j.cnki.syfjx.20230353.
[51] J. Huang, J. Liao, W. Liu, et al., Metabolic composition analysis of mullein isoflavone glycosides in rat serum based on UPLC/ESI-Q-TOF-MS technique, Guangdong Chemical 44 (9) (2017) 50–77.
[52] L. Xie, Q. Huang, B. Yang, et al., Differential chemical composition of Pueraria Mirifica from different varietal sources analyzed based on UPLC-Q-TOF-MS technology, Chinese Journal of Experimental Formulary 27 (19) (2021) 149–156, https://doi.org/10.13422/j.cnki.syfjx.20210847.
[53] S. Tang, X. Li, L. Ma, et al., Study on the chemical constituents of flavored Astragalus and gui zhi Wu Wu Wu Tang based on HPLC fingerprinting and LC-Q-TOF/MS, Chinese herbal medicine 54 (3) (2023) 711–721, https://doi.org/10.7501/j.issn.0253-2670.2023.03.005.
[54] D. Zhen, Y. Huang, X. Lu, et al., Discussion of anti-inflammatory and analgesic substances and mechanism of action of aqueous extracts of Cornus sativus based on UPLC-Q-TOF-MS and network pharmacology, Chinese herbal medicine 54 (12) (2023) 3903–3910. https://doi:10.7501/j.issn.0253-2670.2023.12.017.
[55] M. Zeng, N. Shen, S. Wu, et al., Analysis of the chemical composition of Trifolium pratense based on UPLC-Triple-TOF/MS approach, Chinese herbal medicine 48 (5) (2017) 874–883. https://doi:10.7501/j.issn.0253-2670.2017.05.006.
[56] Y. Guan, X. Zheng, M. Yan, et al., Ultra-performance liquid-liquid-mass spectrometry analysis of the active ingredients of Scutellaria baicalensis-sophora medicinal pairs and their network pharmacology in the treatment of chronic kidney disease, Chinese herbal medicine 53 (20) (2022) 6388–6400. https://doi:10.7501/j.issn.0253-2670.2022.20.011.
[57] D. Zheng, W. Wei, J. Huo, et al., Serum pharmacochemistry of qi FengFuXiao granules based on UPLC-Q-TOF-MS technique, Chinese herbal medicine 52 (3) (2021) 643–652. https://doi:10.7501/j.issn.0253-2670.2021.03.006.
[58] Z. Qu, L.T. Luo, W.J. Zhang, et al., Exploration of the potential pharmacodynamic substances and mechanism of action of Schisandra garcinia cambogia in hepatoprotection based on UPLC-Q-TOF-MS/MS and web-based pharmacological approach, Chinese herbal medicine 53 (8) (2022) 2407–2416. https://doi:10.7501/j.issn.0253-2670.2022.08.018.
[59] C. Yang, X. Zhu, H. Wan, et al., Gray correlation analysis-based study on the spectral-effect relationship between the sedative-hypnotic effects of fried sour jujube nut, Chinese herbal medicine 52 (17) (2021) 5267–5274. https://doi:10.7501/j.issn.0253-2670.2021.17.019.
[60] Z. Liang, Y. Pan, L. Qiu, et al., Changes of chemical components during the nine-steaming and nine-sunning preparation of Rhizoma Polygonati Odorati based on UPLC-Q-TOF-MS/MS analysis, Chinese herbal medicine 53 (16) (2022) 4948–4957. https://doi:10.7501/j.issn.0253-2670.2022.16.004.
[61] C. Wang, Establishment of UPLC-MS/MS method and pharmacokinetic study of reserpine and its 8-0-methyl metabolite in rat plasma. https://link.cnki.net/doi/10.27215/d.cnki.glzyu.2022.000050, 2022.